General Disclaimer

One or more of the Following Statements may affect this Document

- This document has been reproduced from the best copy furnished by the organizational source. It is being released in the interest of making available as much information as possible.

- This document may contain data, which exceeds the sheet parameters. It was furnished in this condition by the organizational source and is the best copy available.

- This document may contain tone-on-tone or color graphs, charts and/or pictures, which have been reproduced in black and white.

- This document is paginated as submitted by the original source.

- Portions of this document are not fully legible due to the historical nature of some of the material. However, it is the best reproduction available from the original submission.

Produced by the NASA Center for Aerospace Information (CASI)

NASA-CR-135350

EPITAXIAL SOLAR-CELL FABRICATION, PHASE II

R. V. D'Aiello, P. H. Robinson, and H. Kressel
RCA Laboratories
Princeton, New Jersey 08540

NOVEMBER 1977
FINAL REPORT for the period 11 November 1974 to 10 June 1977

Contract No. NAS3-19401

Prepared for
Lewis Research Center
National Aeronautics and Space Administration
Cleveland, Ohio 44135

TABLE OF CONTENTS

iii/iv

LIST OF ILLUSTRATIONS

LIST OF ILLUSTRATIONS (Continued)

LIST OF ILLUSTRATIONS (Continued)

LIST OF TABLES

EPITAXIAL SOLAR CELL FABRICATION, PHASE II

by

R. V. D'Aiello

RCA Laboratories
Princeton, NJ   08540

SUMMARY

The research described in this report was conducted during the
second year of a continued study of the growth and fabrication of epi-
taxial silicon solar cells. The major elements of this work consisted
of experimental studies of the epitaxial growth of base-layer and
surface-layer profiles with the goal of identifying structures which
yield the highest solar-cell parameters while maintaining suitability
for use in a space environment.

Dichlorosilane (SiH_2Cl_2) was used as the silicon source material
in all of the epitaxial growths. Both $n/p/p^+$ and $p/n/n^+$ structures
were studied; this included an evaluation of the cell performance of
structures with uniformly doped base layers and base layers containing
exponential doping gradients. Separate studies were conducted of the
effect of a variety of surface layers in conjunction with selected base
layers. Extensive use of secondary ion mass spectroscopic (SIMS) tech-
niques was made in the evaluation of surface-layer profiles (see Appendix
A). Spreading resistance and capacitance-voltage (C-V) analyses were
used to determine base-layer and junction profiles. Correlations were
made between the measured profiles and the solar-cell parameters, es-
pecially cell open-circuit voltage.

It was found that in order to obtain consistently high open-circuit
voltage, the epitaxial techniques used to grow the surface layer must be
altered to obtain very abrupt doping profiles in the vicinity of
the junction. With these techniques, it was possible to grow reproduc-
ibly both $p/n/n^+$ and $n/p/p^+$ solar-cell structures having open-circuit

voltages in the 610- to 630-mV range, with fill-factors in excess
of 0.80 and AM-1 efficiencies of ∿13% (AM-0 ∿ 11.5%).

Combinations and comparisons of epitaxial and diffused surface
layers were also made. Using such surface layers, we found that the
blue response of epitaxial cells could be improved, resulting in AM-1
short-circuit current densities of ∿30 mA/cm^2 (AM-0 values of ∿36
mA/cm^2). The best cells fabricated in this manner had AM-1 efficiency
of 14.1%.

SECTION I

INTRODUCTION

The work reported here has been conducted during a continuation (second year) of research and development devoted to the study of silicon epitaxial solar-cell structures. During the first year of NASA-Lewis sponsorship, the material and electronic properties of epitaxial layers were studied, and it was found that the epitaxial methods used produced silicon layers and junctions that satisfy the basic requirements for efficient solar-cell operation (ref. 1). The most successful solar cells were fabricated by the reduction of dichlorosilane to grow p and n layers on heavily doped substrates. The best performance was obtained from a $p^+p/n/n^{++}$ structure grown with an exponential grade in the n-base layer. This cell had an AM-1 efficiency of 12.5% with an open-circuit voltage (V_{oc}) of 636 mV (ref. 2). The major conclusion of the first year's work was that the epitaxial layers and junctions result in excellent electrical junction characteristics which in turn yield high open-circuit voltage and good fill-factor.

The objective of the second-year continuation is to study in detail the effects of doping gradients grown in both the base layer and surface layer of epitaxial cell structures on solar-cell performance, in particular the open-circuit voltage. Both $n/p/p^+$ and $p/n/n^+$ structures were studied; however, more emphasis was placed on the $n/p/p^+$ cells because of their proven radiation resistance in space applications. A major goal of this work is to demonstrate the reproducible growth of solar-cell structures having high open-circuit voltage $(V_{oc} \sim 700$ mV) in conjunction with high efficiency (AM-0 $\sim$ 15%).

The approach taken was first to study the effect of variations in the base-layer profiles with the surface-layer properties held fixed. Structures were grown with variations thickness, doping level, and

3

selected exponential doping gradients, in order to find an optimized base layer with regard to open-circuit voltage.

This was followed by an experimental study of thin surface layers on optimal base layers. Although the major emphasis was on epitaxially grown surface layers, some comparisons were made with surface layers formed by diffusion. In this work, an analytical technique based on secondary ion mass spectroscopy was found quite useful for the measurement of surface-layer profiles. This allowed correlation between cell performance and surface-layer profiles.

This final report describes the research performed during the period 9 July 1976 to 10 June 1977.

SECTION II

EXPERIMENTAL METHODS

A. Epitaxial Growth Techniques

High-purity dichlorosilane was used as the silicon source material for the epitaxial growth results described in this report. Epitaxial growth of solar-cell structures offers the following unique advantages:

(1) The flexibility of the epitaxial method readily allows for the growth of tailored profiles.

(2) It is the only practical and reproducible method for producing impurity gradients in the base layer of solar-cell structures.

(3) Excellent quality junction results from the *in situ* growth of both junction layers.

(4) In particular, the use of dichlorosilane allows for the rapid growth of the entire structure at a reduced temperature compared with the more commonly used silicon tetrachloride source material (i.e., a 100-µm structure can be grown in ~15 min).

(5) Epitaxial growth has been shown to produce layers with sufficient minority carrier lifetime to satisfy solar-cell requirements.

(6) In the epitaxial method the control of the doping gas flow can readily be accomplished by an electronic-automated system.

(7) By growth of epitaxial layers on highly doped substrate, the "back surface field" is automatically formed at the substrate-epitaxial interface and the thickness of the base layer is readily adjustable to the desired value.

A standard horizontal epitaxial reactor was used. The quartz tube had a cross section of 2 by 4 in. and held a silicon carbide-coated graphite susceptor that was 12 in. long. Heating was accomplished by rf induction into the susceptor, which was inclined with respect to the

horizontal, while the walls of the reactor were cooled by air jets.
All of the gases were metered into the system from a control panel
which provided automatic timing of the duration of each run. Tank
hydrogen was purified by passing it through a Deoxo unit, then a
Pd-Ag diffusion cell. The doping gases used were either arsine or
diborane diluted with hydrogen at the 10- to 20-ppm level and were
further diluted with hydrogen as needed before being metered into the
reactor. Dichlorosilane was metered as a gas directly from the cyl-
inder, and temperatures were measured using an optical pyrometer of
the disappearing filament type. The silicon substrates were cleaned
in megasonic peroxide-ammonia and peroxide-hydrogen chloride solutions
prior to insertion into the reactor and were further cleaned *in situ*
by etching with gaseous hydrogen chloride at high temperature just
prior to growth. Most of the layers were grown at a growth rate of
5 μm/min; however, growth rates of 1 μm/min were used for the 1-μm top
junction layers. The graded layers were grown by changing the doping
flows and, hence, the carrier concentration during growth. Growth
temperatures ranged between 1090 and 1150°C, depending on desired con-
ditions.

B. Solar-Cell Fabrication

In this section, the details of the solar-cell fabrication starting
from as-grown epitaxial wafers are described.

1. General Procedures

The general procedures for fabrication of the solar cells and test
structures are:

(1) Grow epitaxial layers - 3 wafers/run.
(2) Characterize spreading resistance.
(3) Clean wafers - H_2SO_4:H_2O_2; H_2O_2:NH_3OH; H_2O_2:HCl boiling
    solutions.

(4) Metallize by evaporation of Ti/Ag (0.2 μm/3 μm) through metal mask on front, Ti/Ag on back.

(5) Spin-on AR coating – bake and sinter.

(6) Screen-on wax to define cell and test structure areas.

(7) Etch silicon to form mesa structures delineating cell area.

(8) Remove wax, rinse, and bake.

These processing steps are described in more detail below.

2. Mask Design

The contact mask used to delineate the metallization pattern for all cells reported here is shown in figure 1. The large cell is 2 x 2 cm, having 11 current collecting fingers and a single bus-bar with a total 7% metal area coverage. The two small cells and ten diodes are for diagnostic purposes such as the measurement of lifetime and area dependence of electrical characteristics. The parallel bar structures A and A' are included for measurement of surface-layer sheet resistance and metal-to-silicon contact resistivity, and the line structure B is for the measurement of metal sheet resistance.

3. Metallization

Metallization was done by E-gun evaporation of 0.2 μm of titanium followed by 3 μm of silver. These metals are evaporated through a 5-mil-thick Be-Cu mask with the contact pattern (shown in figure 1) etched into it. The silicon substrates were not heated during evaporation; sintering was done in a separate furnace at 500°C for 15 min in argon.

4. Antireflection Coating

A commercially available* titaniumsilica film spin-on antireflection (AR) coating was used because of its ease in handling and good optical

---

*Titaniumsilica film-type C, purchased from Emulsitone Co., Whippany, NJ.
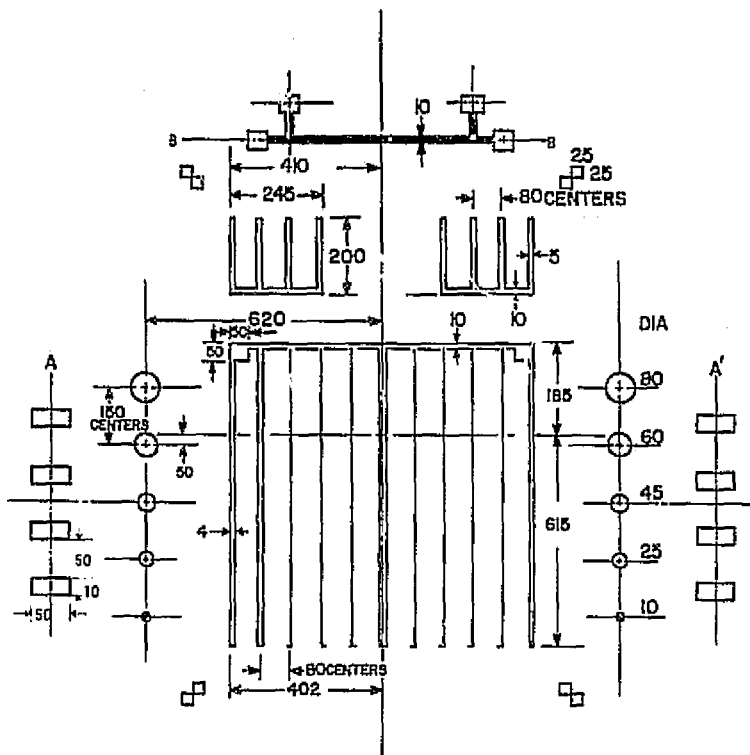
Figure 1. Solar-cell mask design including
diagnostic cells.

properties. The type-C spin-on film we purchased and used has a reported
index of refraction of 1.96. The liquid is spun onto the silicon wafer
and then baked successively at 200°C and 400°C for 15 min in air. The
resulting thickness of the film depends upon the spin-speed, but satu-
rates at ~765 Å for spin speeds greater than 6000 rpm.

   In order to obtain thinner films with lower spin speeds, the liquid
was diluted 75% liquid to 25% ethyl alco. l. With this solution, a spin
speed of 4100 rpm yields a reproducible film thickness of 750 Å. The
optical reflection and transmission properties were measured over the
visible wavelength range. The measured reflection of a typical spin-on

AR coating on a polished silicon surface is shown in the upper trace
of figure 2. By making transmission measurements of similar films on
quartz plates, absorption was estimated at less then 1% for wavelengths
greater than 4000 Å and only 5% at 3500 Å. The measured absorption is
shown in the lower trace in figure 2.
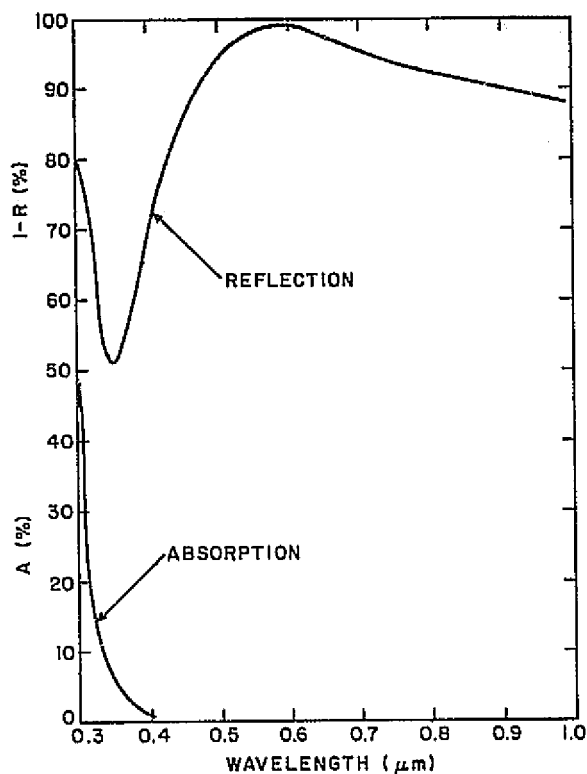
Figure 2. Reflection and absorption properties of spin-on
titaniumsilica film as a function of wavelength.

5. Mesa Etching

We use mesa etching to define the cell and test structure areas and
to delineate and clean the peripheral junction areas. This is accom-
plished by screening a presoftened wax onto the wafers through a metal
mask. The exposed silicon is then etched to a depth of 1 mil (25 μm)

using a hydrofluoric acid, acetic acid, nitric acid (1:2:2) solution. The resulting cell area varies somewhat from run to run but is generally close to 4.4 cm^2. This process results in a clean, damage-free peripheral mesa area including the junction at the cell edge.

C. Solar-Cell Measurements

Indoor testing of the cells was conducted with the apparatus shown in figure 3. The GE ELH lamp was calibrated for spectral output at regulated lamp voltages of 90, 100, and 110 V using an EG&G PV 444A photodetector and narrow-band optical filters at a distance of 30.5 cm. Response curves taken at each voltage compared with an approximate AM-1 spectrum are shown in figure 4.

The output was also measured as a function of distance from the lamp over the 10- to 60-cm range and was found to vary as one over the distance squared, as expected. This would allow for measurement of cells at different intensities with the same spectral content.

For solar-cell measurements, it was decided to operate the lamp at 100 V to prolong the lamp life (expected life at 110 V is 30 h). At 100 V, we have experienced lamp life from 50 to 100 h. The integrated spectral power at a distance of 30.5 cm, when operating at 100 V, is 99 mW/cm^2. However, the lamp output, when compared with the AM-1 spectrum, is higher in the orange-red and lower in the blue-violet.

The cell holder shown in the inset of figure 3 is a gold-plated copper block with holes for vacuum hold-down of solar cells. For temperature stability a thermoelectric cooler and cooling fins (not shown) are mounted on the rear of the block. The fingerclip arrangement is a balanced current, modified (common-ground) four-point contact. The balanced current contacts to each end of the cell cancel bus-bar voltages and tend to keep the current distribution uniform over the cell area.

The dynamic load shown is used to measure cell current and provide offset voltages for open-circuit and short-circuit current measurements.

10
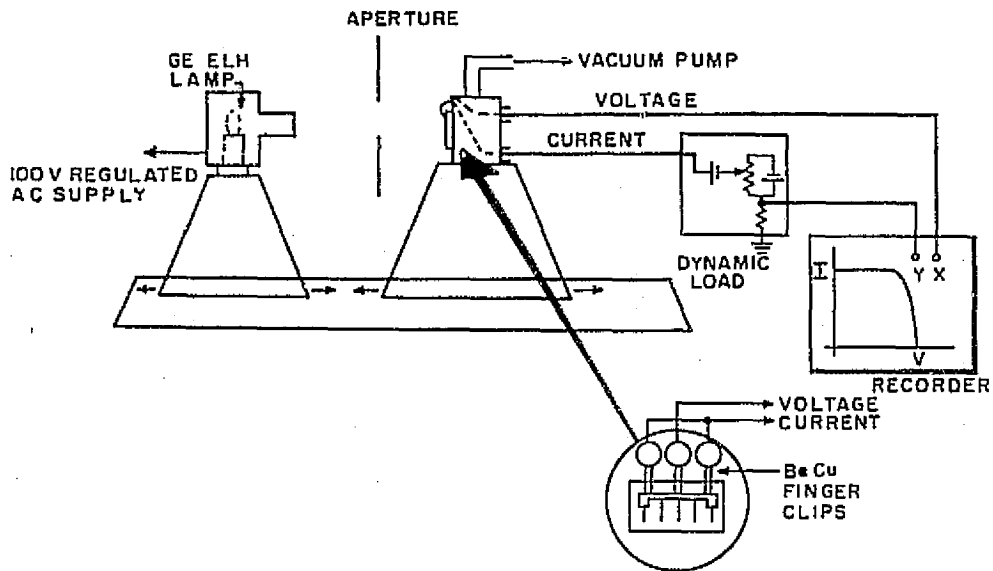
Figure 3.   Solar AM-1 simulator and cell mount.
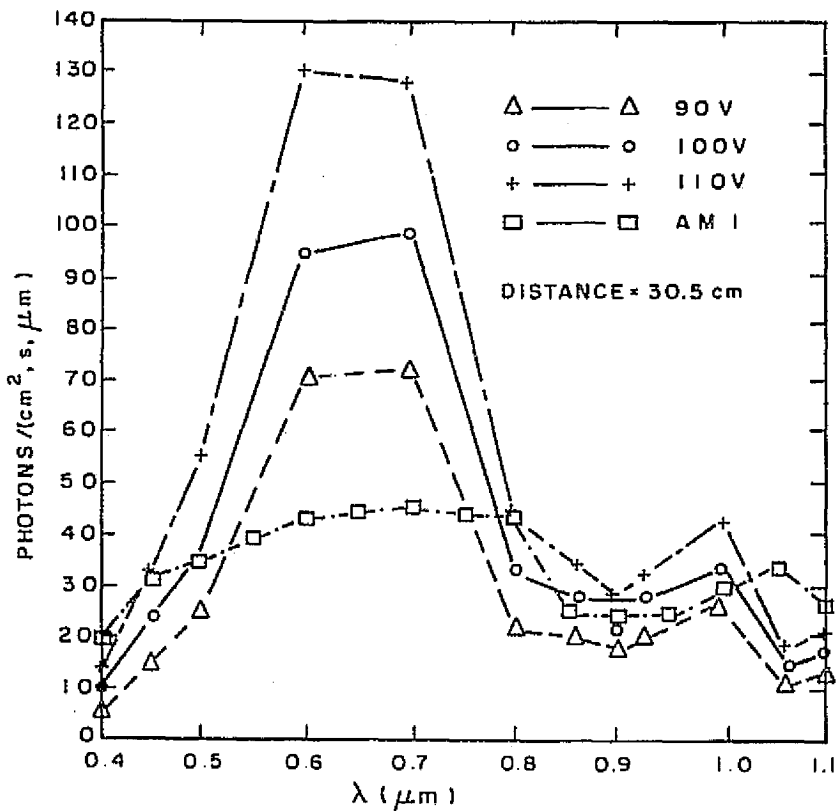
Figure 4.   Output response curves for GE ELH lamp compared
with simplified AM-1 spectrum.

11

For calibration purposes a secondary standard cell provided by the NASA-Lewis Research Center was measured prior to each run. Measurements were made at 27°C.

Spectral response measurements were made by inserting a filter wheel containing narrow-band calibrated optical filters between the lamp and detector. To determine quantum efficiency (electron/incident photon), the light is chopped at 520 Hz, and the voltage developed across a 100-Ω load in parallel with the detectors is measured as a function of wavelength using a lock-in amplifier. The detector used was an EG&G PV 444-A photocell, supplied with certified quantum efficiency. The quantum efficiency of solar cells was obtained by taking the ratio of the voltage developed across the test cell at each wavelength to the voltage of the EG&G PV 444-A detector.

Outdoor testing was conducted on the roof on very clear days by using a calibration procedure similar to that described above and in NASA TM X-71771, 1975.

A comparison of the AM-1 simulation and some outdoor testing results with NASA-Lewis measurements on our epitaxial cells is given in Appendix D.

SECTION III

SOLAR-CELL PERFORMANCE

A. Base-Layer Profile Studies

1. Uniformly Doped Base Layers

In order to form a baseline for later comparison with graded base structures, a set of uniformly doped p-base layer cell structures was grown. Four different $n^+/p/p^+$ profiles were grown having ~ 70-μm-thick p-base layers boron doped at 10^{14}, 10^{15}, 3×10^{16}, and 10^{17} A cm^{-3}, all grown on 1×10^{19} A cm^{-3} (boron), <100>, p^+ substrates. The surface n-layers in each case were grown 1.5 μm thick, doped with arsenic to 1×10^{18} A cm^{-3}.

The AM-1 illuminated cell characteristics and junction parameters are summarized in table 1 in which, for purposes of the analysis and discussion to follow, the base-layer diffusion constant, D, was taken from the literature (ref. 3), and the diffusion lengths calculated from $L = \sqrt{D\tau}$ are also listed. For an interpretation of the measured variation of open-circuit voltage, V_{oc}, the back-surface-field (BSF) effect (refs. 4,5) and light-generated carrier flooding (ref. 6) in the base must be considered. The latter effect is especially important in sample 766531 which has the lowest base-layer doping level, but is negligible in the other samples. Although we do not have a complete understanding of the BSF enhancement of V_{oc} at present, this effect is expected to be prevalent in samples having $L/W \gtrsim 1$ and to depend on the detailed parameters of the back-surface region (ref. 7). For these epitaxial structures, the back-surface-field arises from the high-low p^+-p junction which occurs over a region of 5 to 8 μm at the base-substrate interface.

We assume that this interface region is characterized by a back-surface recombination velocity, S_B, and a photogenerated potential

TABLE 1. SUMMARY OF EPITAXIAL CELL PARAMETERS,
UNIFORMLY DOPED BASE LAYERS

| | AM-1 Parameters | | | | | Junction Parameters | | | |
Cell/Base Doping	J_{sc} (mA/cm^2)	V_{oc} (mV)	F.F. --	η (%)	R_s (Ω)	n --	J_o (A/cm^2)	τ (μs)	L (μm)[b]
766531/10^{14}	26.4	550	0.63	9.5	1.8	1.6[a]	4.5 x 10^{-8}	9	165
768089/1 x 10^{15}	24.9	530	0.760	10.5	0.22	1.00	5 x 10^{-11}	1.8	77
767881/3 x 10^{16}	25.6	588	0.720	11.3	0.48	1.03	1.1 x 10^{-11}	1.3	55
768940/1 x 10^{17}	24.6	601	0.795	12.3	0.24	1.00	1.7 x 10^{-12}	0.75	34

[a] High n-factor due to conductivity modulation in the 10^{14} A cm^{-3} base.
[b] Diffusion length L calculated from $L = \sqrt{D\tau}$.

ΔV_{BSF}(ref. 8). As a first approximation, if it is assumed that $S_B = 0$, and contributions from the surface n-layer are neglected, then the open-circuit voltage V_{oc} can be written as

$$V_{oc} = \frac{kT}{q} \left[\ln \left(\frac{J_{sc}}{J_o} \right) + \ln \coth \left(\frac{W}{L} \right) \right] + \Delta V_{BSF} \qquad (1)$$

where J_{sc} is the short-circuit, solar-generated current density, W is the base width, L is the minority carrier diffusion length in the base, and J_o is the dark saturation current density given by

$$J_o = \frac{q\, n_i^2}{\left(N + \frac{J_{sc} \cdot \tau}{qW} \right)} \quad \frac{D}{L} \qquad (2)$$

where n_i is the intrinsic carrier density for silicon, nominally[*] taken as 1.5×10^{10} A cm^{-3}, N is the doping concentration in the base, τ is the minority carrier lifetime, and D is the diffusion constant.

---

[*]If bandgap shrinkage is important at the higher doping levels, n_i becomes a function of the doping level and J_o can be considerably increased (refs. 9,10).

Equation (1) with ΔV_{BSF} taken equal to zero is plotted in figure 5 along with the measured values of V_{oc}. It is seen that a back-surface-field voltage contribution appears to be present and that its value diminishes as the base-layer doping increases. One possible reason for this is that the ratio of the doping level in the substrate (1×10^{19} A cm^{-3}) to that in the base layer decreases from 10^5 to 10^2 in these samples, thereby reducing the Fermi level difference, resulting in a diminished back-surface-field effect. In addition, there is slight evidence of open-circuit voltage saturation at the highest base-layer doping level ($N = 10^{17}$ A cm^{-3}) explored in this experiment.
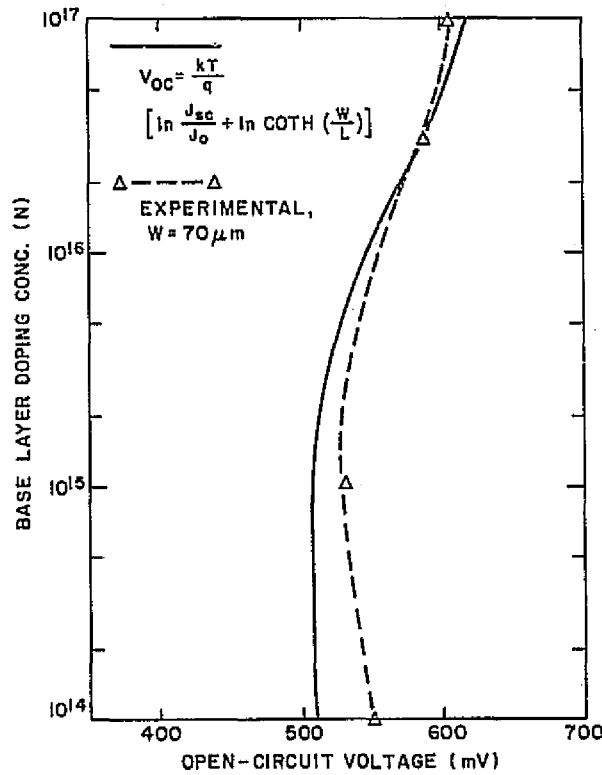
Figure 5. Calculated (Eq. 1) open-circuit voltage and experimental values for the samples of Table 1.

To further explore the effect of base-layer doping on open-circuit voltage, a set of experiments was conducted by growing both $p/n/n^+$ and $n/p/p^+$ structures in which two uniform base-layer doping levels were used, namely, 1×10^{16} and 1×10^{18} A cm^{-3}. Typical spreading resistance traces for these samples are shown in figures 6, 7, and 8. A summary of the solar-cell and junction performance parameters is given in table 2.
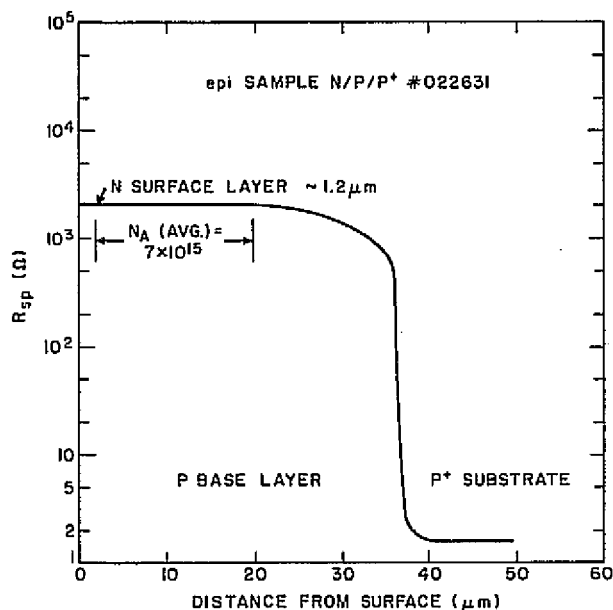
Figure 6. Spreading resistance trace of the base-layer for sample 022631 of table 2.

The base-doping levels of 10^{16} and 10^{18} A cm^{-3} were chosen first because they are in the range where the highest open-circuit voltage is expected, and, second, two orders of magnitude difference in doping level is expected to produce large differences in V_{oc}. The measured open-circuit voltages given in table 2 do not exhibit this expected large difference but rather only modest increases in V_{oc} are observed
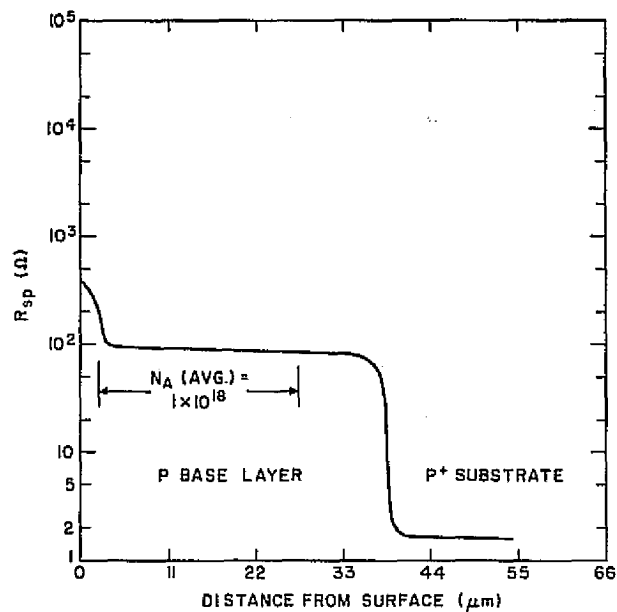
Figure 7. Spreading resistance trace of the base-
layer for sample 022271 of table 2.
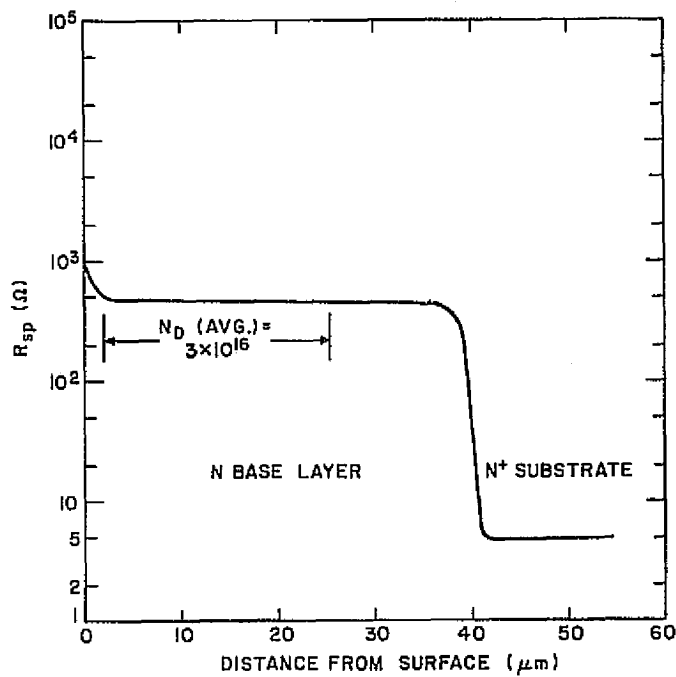
Figure 8. Spreading resistance trace of the base-
layer for sample 024713 of table 2.

17

TABLE 2. SUMMARY OF BASE-LAYER PROFILES AND CELL CHARACTERISTICS
FOR STRUCTURES HAVING HIGHLY DOPED BASE LAYERS

| | Base-Layer Profile | | | AM-1 Parameters | | | | Junction Parameters | |
| | Doping (A/cm^3) | Thickness (μm) | Substrate — | J_{sc} (mA/cm^2) | V_{oc} (mV) | F.F. — | η (%) | n — | J_o (A/cm^2) |
Sample – Type									
022631, n/p/p^{++}	1×10^{16},B	37	10^{20},B	27.5	540	0.760	11.7	1.00	2.3×10^{-11}
022271, n/p/p^{++}	1×10^{18},B	38	10^{20},B	23.5	580	0.772	10.6	1.00	4.2×10^{-12}
024713, p/n/n^{++}	3×10^{16},As	40	10^{20},P	27.1	600	0.765	12.7		
025943, p/n/n^{++}	7×10^{17},As	55	10^{20},P	26.1	610	0.800	13.5		
024513, p/n/n^{++}	4×10^{16},As	55	10^{20},P	29.5	590	0.790	14.1		
022963, p/n/n^{++}	1×10^{18},As	63	10^{20},P	26.0	602	0.778	12.5		

at the higher doping levels. Open-circuit voltage saturation with increasing base-layer doping level has been reported (ref. 11) previously and several theories have been proposed to explain this result (refs. 12, 13). No attempts were made to distinguish among these theories using the present samples; however, several additional possibilities arise, and must be considered in the case of epitaxially grown structures. First, for the samples with highly doped ($\sim 10^{18}$ A cm^{-3}) base layers, the properties of the surface layer become important since the doping level in the surface layer is comparable to that of the base. For similar recombination lifetimes, dark currents contributed by the surface layer can be comparable to or even larger than those in the base. In addition, recombination currents contributed by the surface can further increase the total dark current, thereby lowering the open-circuit voltage. Some experimental evidence supporting this view is given in Appendix C.

Another condition which can lead to open-circuit voltages which are lower than expected is a reduction of the base-layer doping level immediately adjacent to the junction. This usually occurs just prior to and during the growth of the top layer, and results from two mechanisms, outdiffusion of base dopant (especially boron) in the gas stream during the flush cycle after the growth of the base layer and thermal diffusion during the growth of the top layer.

To explore this possibility, a C-V analysis was done on samples 022631 and 022271 of table 2. These C-V plots are shown in figures 9 and 10 with data also shown in figure 9 for a typical n$^+$/p diffused junction cell. The two distinct slope regions show that for the epitaxial structures the profiles are graded with the doping level decreased near the junction. This is especially true for the more highly doped sample of figure 10. The net result is that for these two epitaxial samples, a difference of only one order of magnitude in doping level instead of two was actually obtained. This brings the difference in measured open-circuit voltage between these samples closer to what might be expected. However, for the samples with higher doped base
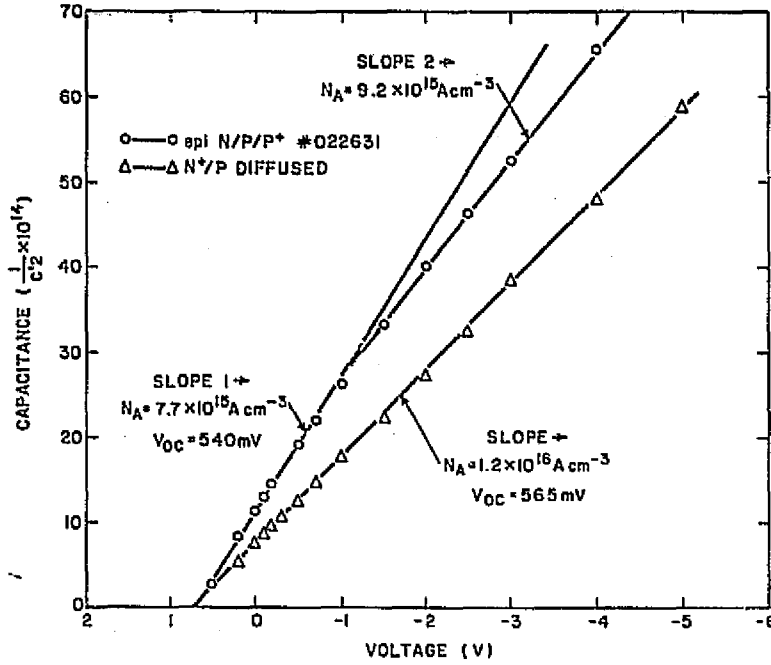
Figure 9. Capacitance-voltage plots for epitaxial sample 022631 of table 2 and for a typical diffused junction n$^+$/p solar cell.
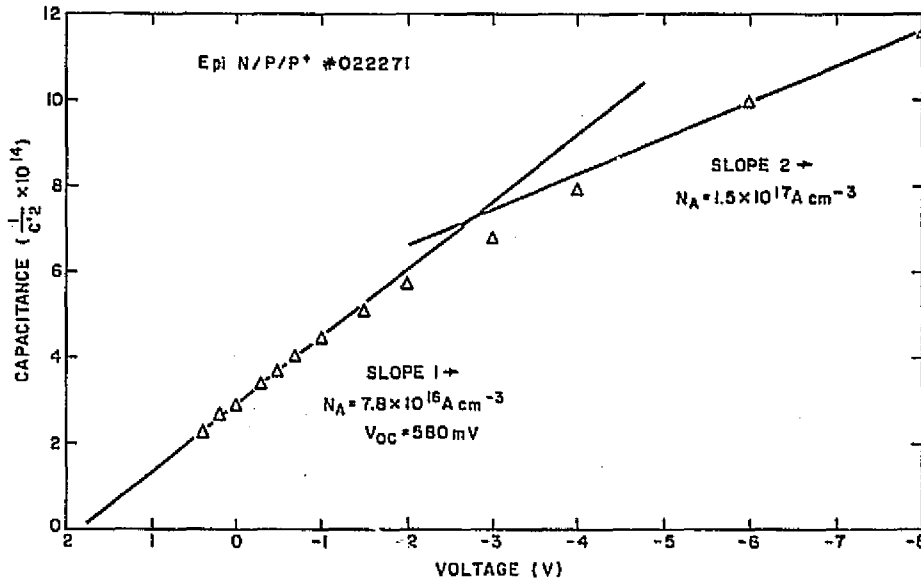
Figure 10. Capacitance-voltage plot for epitaxial sample 022271 of table 2.

layers, there is some additional lowering of V_{oc}, perhaps due to a dark current contribution from the surface layer.

The illuminated and dark electrical characteristics of these samples remain quite good even at the highest doping levels. In particular, generally good fill-factors of 0.76 to 0.80 are obtained. These high fill-factors are related to the quality of the p/n junction formed by epitaxy.

2. Graded-Base Epitaxial Structures

Initial experimental studies of graded-base structures were conducted on $n/p/p^+$ structures. The p-base layers were grown with an approximate exponential grade, accomplished by continuously decreasing the boron content in the gas stream. The top n-layers were grown as described for the case of uniform base structures.

The base-layer profiles for three such structures are shown in figures 11, 12, and 13. The "built-in" electric fields calculated
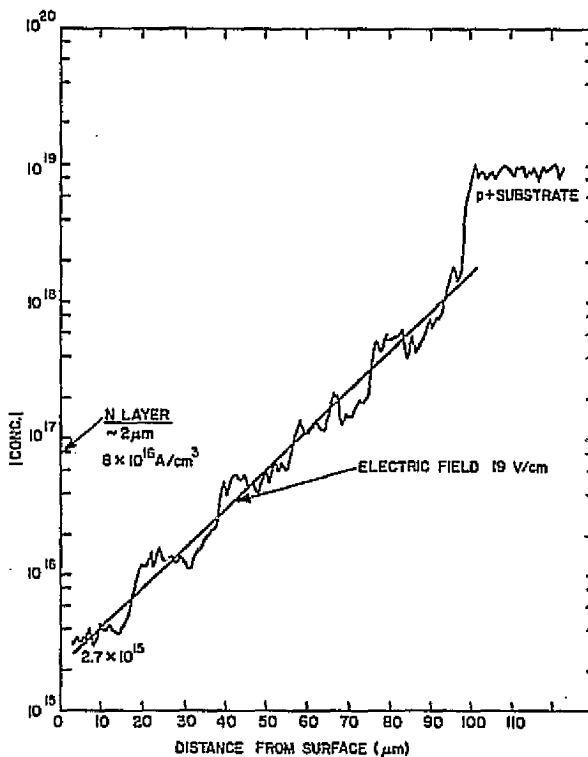
Figure 11.

Concentration profile of epitaxial structure 760984.

21
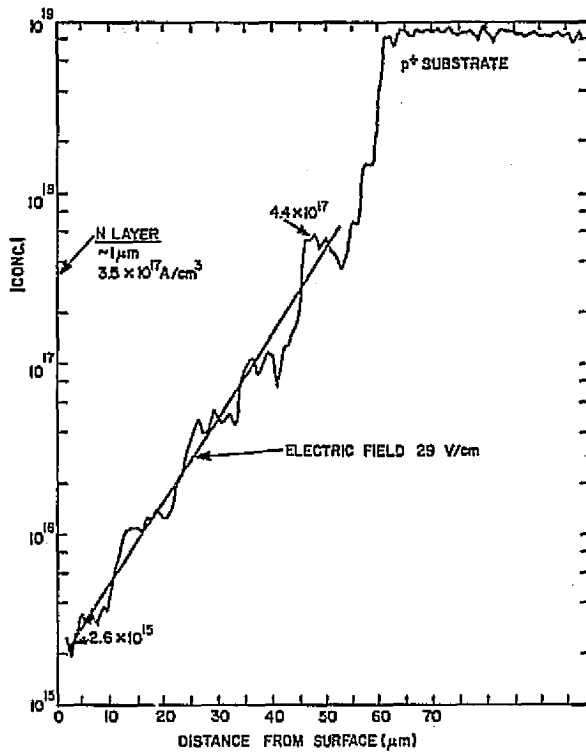
Figure 12.

Concentration profile of epitaxial structure 763088.
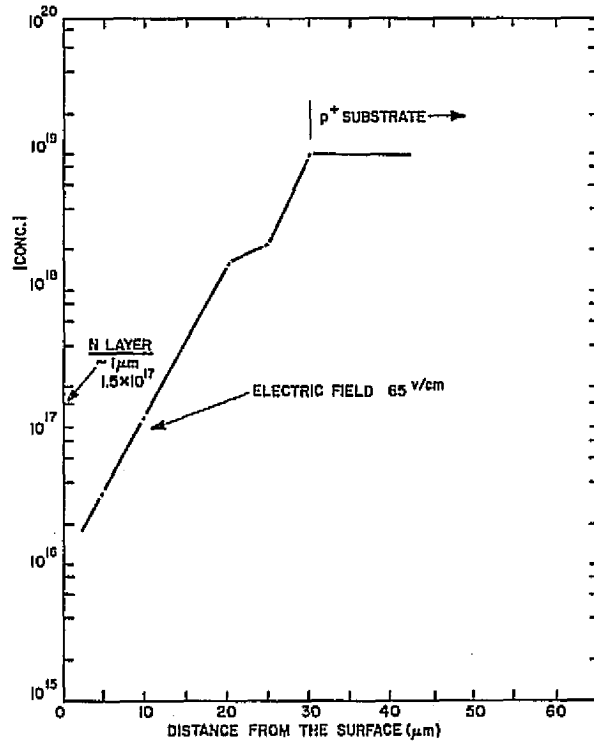
Figure 13.

Concentration profile of epitaxial structure 890229.

22

from the logarithmic slopes associated with each grade are 19, 29, and 65 V/cm as shown in the figures. Solar cells were fabricated from these structures and a summary of the illuminated cell performance and junction parameters is given in table 3.

B. Surface-Layer Studies

1. Introduction

From our studies of epitaxially grown solar-cell structures, we have found that the surface layer plays an important role in determining overall cell performance. In the previous two sections, it was seen that this is especially true for those structures which have the highest open-circuit voltage and thus show promise of the greatest efficiency. These structures make use of highly doped ($\geq 1 \times 10^{17}$ A cm^{-3}) base layers in order to obtain the very low values of saturation current density required for high open-circuit voltage operation.

In order to realize these conditions, the surface layer must contribute lower values of recombination current than the base layer. In addition, for high collection efficiency at short wavelengths, the diffusion length in the surface layer should be greater than its thickness. These conditions, as well as those relating to junction quality, indicate the following general guidelines for the properties of the surface layer:

- Relatively thin ($\lesssim 1$ μm)
- Doping level greater than base layer ($\gtrsim 10^{18}$ A cm^{-3})
- Reasonably long lifetime
- Abrupt, high quality junction
- Low defect density

Also, the incorporation of a doping gradient with doping level decreasing from the surface is beneficial for enhanced carrier collection.

TABLE 3. SUMMARY OF CELL PARAMETERS (AM-1 SIMULATION)

Structure	Field (V/cm)	J_{sc} (mA/cm^2)	V_{oc} (mV)	F.F.	η (%)	$n^{(a)}$	$J_o^{(a)}$ (A/cm^2)	(b) (μs)	R_s (Ω)
Epitaxial n$^+$n/p/p$^+$									
790984	19	25.1	557	0.721	10.3	1.10	6 x 10^{-11}	1.3	1.2
763088	29	29.6	541	0.715	11.8	1.25	2 x 10^{-9}	0.55	0.67
890229	65	30.2	585	0.735	13.0	1.09	3 x 10^{-11}	0.35	0.93
Control n$^+$/p	0	31	560	0.740	13.2	1.08	8 x 10^{-11}	3	0.68

(a) Obtained from measurement of illuminated J_{sc} vs V_{oc} characteristics.

(b) Average of open circuit and reverse recovery on diagnostic diodes.

In the sections which follow, we will describe the approaches used in an attempt to achieve these conditions. In most cases, the epitaxial base layer was 25 to 35 μm thick with a doping profile exponentially graded from $\sim 10^{17}$ A cm^{-3} at the junction to $\sim 10^{18}$ A cm^{-3} near the substrate. This profile was suggested by C. Baraona and C. Swartz (ref. 14). The surface layers studied include those grown epitaxially under a variety of conditions as well as those formed by combinations of epitaxy and diffusion. Our studies of epitaxial surface structures were restricted to relatively thick layers of approximately 1-μm thickness since layers much thinner than this could not be grown reproducibly.

Evaluations included the measurement of solar-cell performance and junction parameters. The shallow surface-layer doping profiles were measured by using a modified Secondary Ion Mass Spectrometer (SIMS) which was built at RCA Laboratories specifically for rapid depth profiling of shallow structures. A description of this instrument is given in Appendix A. At the time this work was conducted, only p-type dopants, boron and aluminum, could be measured with the required sensitivity. Consequently, most of the detailed analysis were conducted on p/n/n$^+$ structures. Solar cells made from n/p/p$^+$ structures were also studied and their behavior did not differ substantially from the p/n/n$^+$ cells.

2. Initial Surface-Layer Studies – p/n/n$^+$ Structures

In our initial studies, the conditions of growth for the surface layer were such that a uniformly doped layer of ~ 1-μm thickness was produced. We have often found that when such surface layers were grown on base layers having a high doping level ($\gtrsim 10^{17}$ A/cm^3), the open-circuit voltage obtained is 600 mV or less, which is considerably lower than expected.

A typical profile measured for one of these structures is shown in figure 14. Two features of this profile are of significance with regard to solar-cell performance. First, the retrograde profile near the
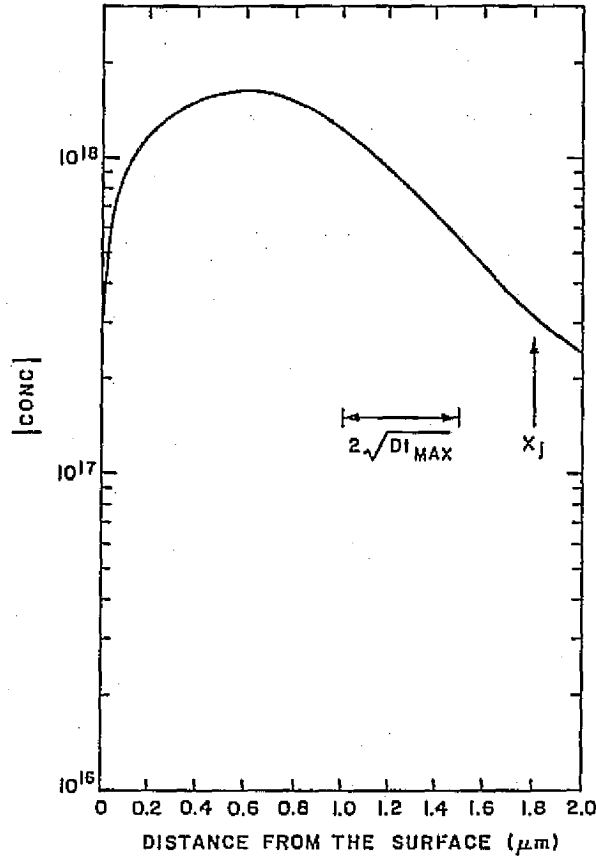
Figure 14. Total boron concentration profile as determined
by SIMS for the surface layer of an epitaxial
$p/n/n^+$ structure.

surface is undesirable since it can cause enhanced carrier recombination at the surface. This surface profile most likely results from the conditions at the end of the epitaxial growth cycle. The gases (hydrogen, dichlorosilane, and diborane) are shut off simultaneously, followed by a 5-minute hydrogen flush cycle at the growth temperature (1150°C). It is likely that during this time, dopant (boron) is lost to the gas stream, or an additional several tenths of a micron is grown with continuously diminished boron concentration. Second, the profile shape near the junction is more graded than expected. The shape of the

profile within 1 μm of the junction appears to result from a combination of diffusion (the maximum estimated diffusion length is 0.5 μm as shown in figure 14) and from a somewhat graded initial growth. The grade in itself is a desirable feature; however, in this case, it results in an electrically graded junction with a lower than expected concentration at the depletion edge in the surface layer. For $p/n/n^{++}$ structures having n-base doping levels of $\geq \sim 4 \times 10^{17}$ A cm^{-3}, the above condition would result in a saturation current density dominated by the surface layer, resulting in a limitation in the maximum attainable open-circuit voltage.

3. Improved Surface-Layer Profiles

Attempts to improve the top layer profile were made in two ways. First, since we believe that most of the gradient in the profile near the junction is due to diffusion, just prior to the growth of the top layer the temperature was dropped from 1150 to 1090°C and maintained at 1090°C during the growth. Also, more diborane than was previously used was added at the beginning of the growth cycle. The results of these experiments and a comparison with a typical previous profile are shown in profiles II and III of figure 15, where curve III results from both a temperature reduction and added diborane level, and curve II from just added diborane but grown at 1150°C. Both profiles show a marked increase in the doping gradient near the junction as well as a large increase in the total boron content of the surface layer.

Second, attempts were made to combine the above techniques with an elimination of the retrograde profile at the surface. This was done by maintaining the flow of diborane for a period of time during the flush cycle at the end of growth. The retrograde was reduced by this technique and could be completely reversed (boron accumulation) by cooling from the growth temperature in the presence of diborane.
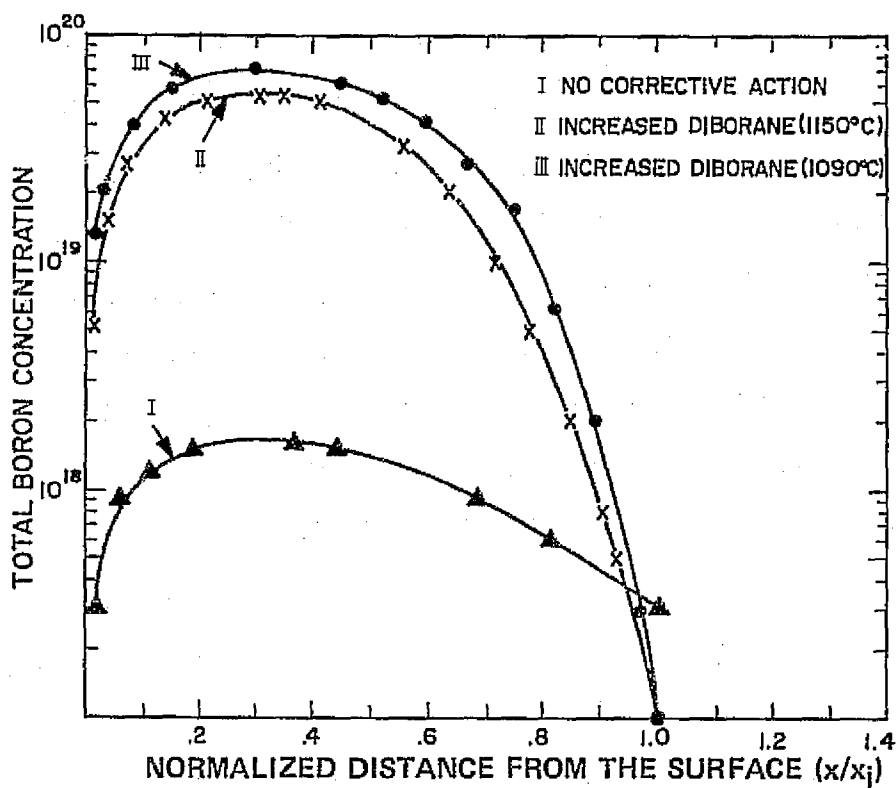
Figure 15. Boron concentration profile determined
by SIMS for surface layers grown under
three different conditions.

4. Solar-Cell Performance with Improved Surface Layers

A number of $p^+/n/n^{++}$ solar cells were fabricated using the tech-
niques described above to grow the top p^+ layer. The details of the
growth conditions, profiles, and the solar-cell responses for these
samples as well as for two samples grown without corrective action are
given in table 4. The surface-layer profiles referred to in the second
column of table 4 are shown in figures 15 through 19. The profile of
figure 19 shows no boron retrograde at the surface, but rather a boron
accumulation near the surface due to changes made in the flush cycle.

Examination of those data shows that the open-circuit voltages are
increased in the samples where some corrective action was taken. The

TABLE 4. RESULTS OF EPITAXIAL SURFACE-LAYER STUDIES – $p/n/n^+$ STRUCTURES

Sample	Surface Layer		Base Layer			AM-1 Parameters			
	Top Layer Profile	x_j (μm)	Description of Base Layer	Base-Layer Doping (A cm^{-3})	Base Thickness (μm)	J_{sc} (ma/cm^2)	V_{oc} (mv)	F.F. —	η (%)
024713	I, Fig. 15	∿0.6	uniform	3×10^{16}	40	24.6	600	0.765	11.5
025943	I, Fig. 15	∿1	uniform	7×10^{17}	55	23.7	610	0.800	11.8
N	II, Fig. 15	∿1.5	graded	$10^{17}/10^{18}$	35[a]	22.7	615	0.784	11.3
B	III, Fig. 15	∿0.7	graded	$8 \times 10^{16}/10^{18}$	45[a]	25.6	620	0.770	12.5
A	III, Fig. 15	∿1.1	graded	$6 \times 10^{16}/10^{18}$	45[a]	22.7	625	0.806	11.8
C1-1	Fig. 16	∿1.1	graded	$4 \times 10^{16}/6 \times 10^{17}$	36	25.8	620	0.810	13.0
C1-3	Fig. 17	∿0.8	graded	$5 \times 10^{16}/9 \times 10^{17}$	28	26.5	627	0.810	13.7
C2-1	Fig. 18	∿1.4	graded	$4 \times 10^{16}/7 \times 10^{17}$	55	21.4	610	0.770	10.3
C3-1	Fig. 19	∿1.2	graded	$3 \times 10^{16}/5 \times 10^{17}$	45	23.4	618	0.802	11.8

(a) Listed value is total grown layer thickness; 25 μm is graded, the remainder is grown at a doping level of 10^{18} A cm^{-3} or a 1×10^{19} A cm^{-3} n^+ substrate.

COSMO C' #1-1

Figure 16. Boron concentration in the top layer determined by SIMS analysis for sample C'1-1.
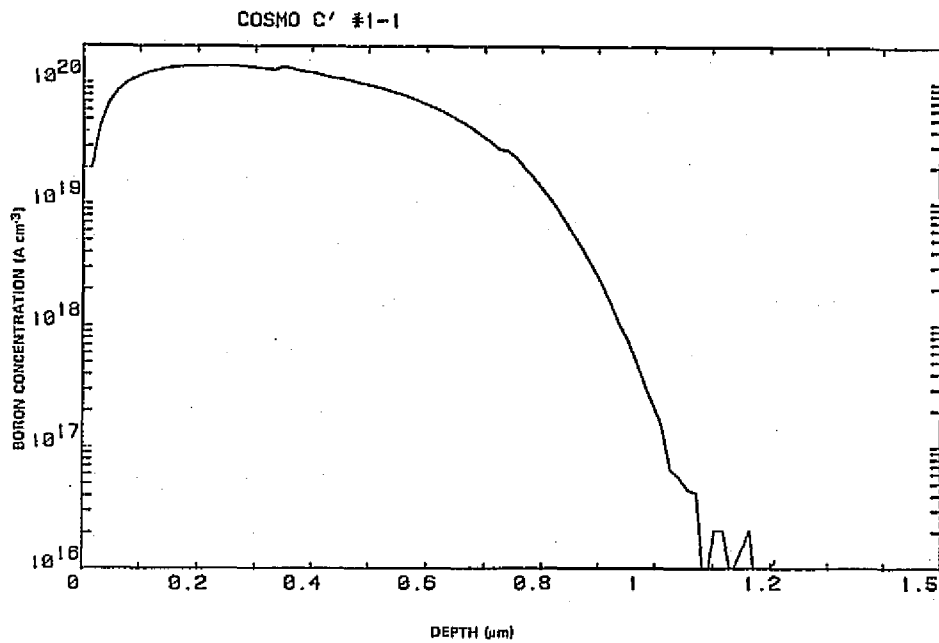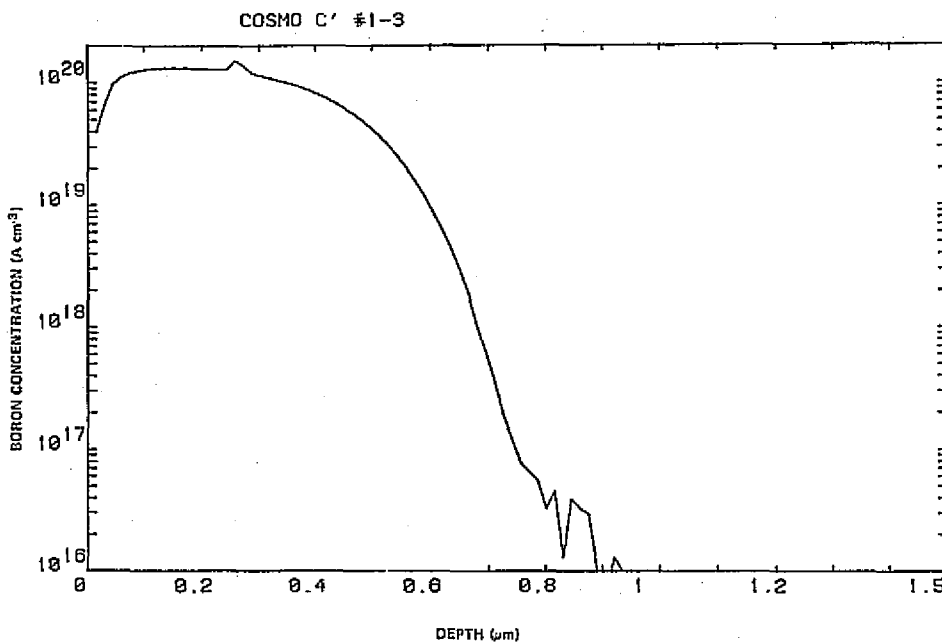
COSMO C' #1-3

Figure 17. Boron concentration in the top layer determined by SIMS analysis for sample C'1-3.

COSMO C′ #2-1
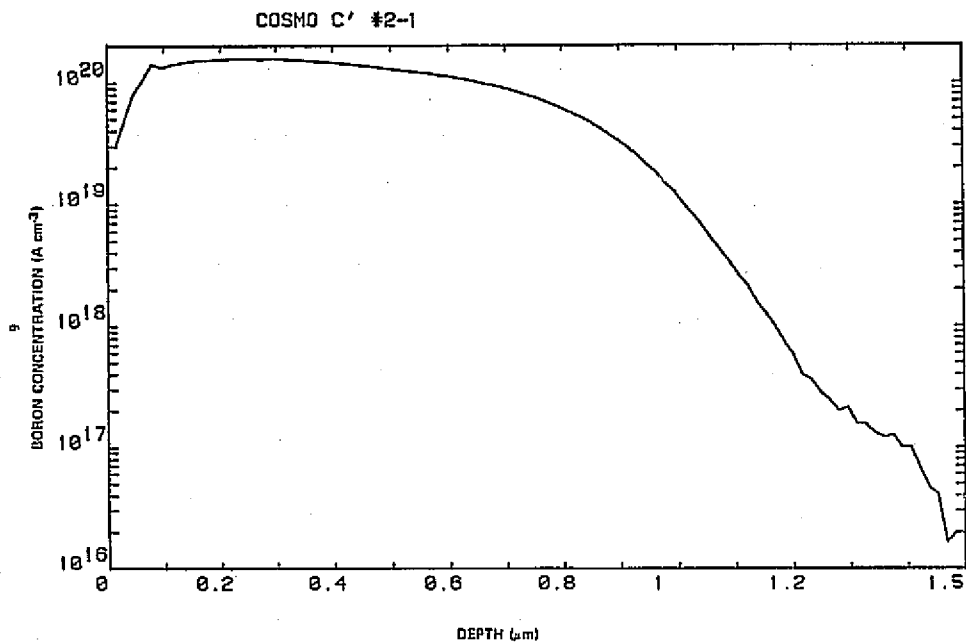
Figure 18. Boron concentration in the top layer determined by SIMS analysis for sample C′2-1.

COSMO C′ #3-1
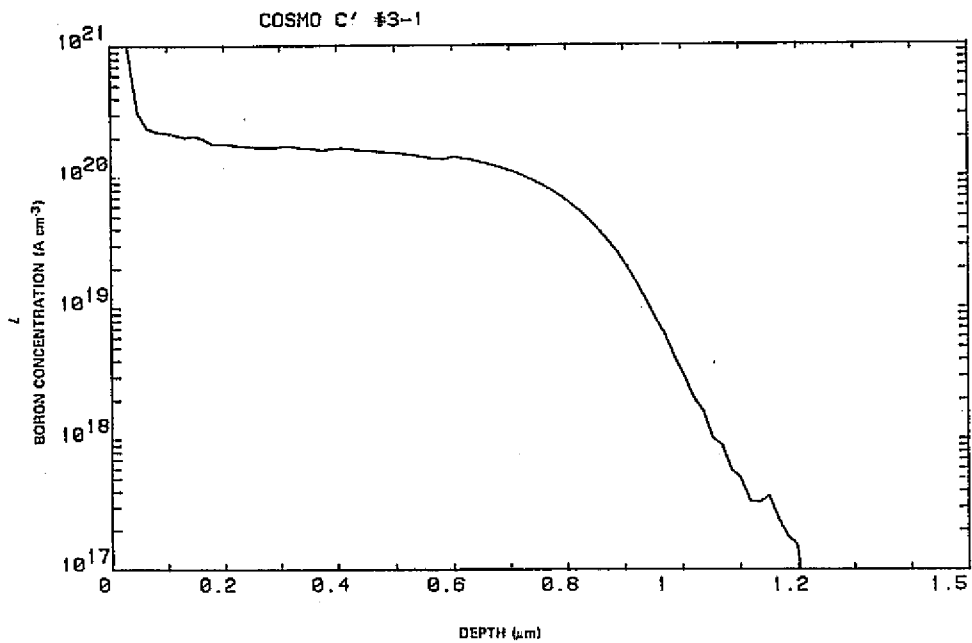
Figure 19. Boron concentration in the top layer determined by SIMS analysis for sample C′3-1.

improvement in open-circuit voltage is typified by samples A and 025943, since the latter sample has ~10 times higher doping concentration in the base layer.

Following is a summary of the $p/n/n^+$ solar-cell characteristics obtained using the above techniques:

- High fill-factors (~80%) related to good junction quality are obtained in most cases.
- The boron surface retrograde can be eliminated and, in fact, reversed (boron accumulation) by proper post-growth techniques; however, no significant improvement in short-circuit current or other cell parameters was noted in these samples.
- The magnitude of the short-circuit current density is low for all samples, but the trend is toward higher values for thinner surface layers.

5. $n/p/p^+$ Structures

We also fabricated $n/p/p^+$ solar cells using epitaxial techniques with profiles similar to those described for the $p/n/n^+$ structures. Structural details and the measured AM-1 parameters are given in table 5, where it can be seen that the performance is similar to the epitaxial $p/n/n^+$ cells.

TABLE 5. SUMMARY OF RESULTS FOR $n/p/p^+$ EPITAXIAL SOLAR CELLS

$n/p/p+$ Cell No.	X_j (μm)	Base Layer		AM-1 Parameters			
		Thickness (μm)	Doping (A cm^{-3})	J_{sc} (mA/cm^2)	V_{oc} (mV)	F.F. —	η (%)
048725	0.9	35	$1 \times 10^{17}/5 \times 10^{17}$	22.8	612	0.795	11.4
052310	1.0	40	$7 \times 10^{16}/5 \times 10^{17}$	20.5	600	0.770	9.8
052180	1.3	50	$1 \times 10^{17}/5 \times 10^{17}$	21.0	615	0.800	10.7

The highest efficiency of the epitaxial cells described in the preceding sections is limited to $\sim$13% AM-1 ($\sim$11% AM-0). These efficiency values were achieved with open-circuit voltage (V_{oc}) $\overset{\sim}{=}$ 625 mV, fill-factor (F.F.) $\overset{\sim}{=}$ 0.80 and short-circuit current density (J_{sc}) $\leq$ 25 mA/cm^2. The major limiting factor for these cells is the low values of J_{sc}, which are generally less than 25 mA/cm^2. The reason for this can be found by examining the spectral response for these cells. A spectral response curve for one of the cells of table 4 is shown in figure 20(a) and (b) along with the illuminated cell parameters. This response curve is typical for these cells and shows that the major limitation in short-circuit current results from low quantum efficiency at wavelengths less than 5500 Å. This type of response is related to the properties of the surface layer since most of the blue response is derived from that layer.

This poor blue response is believed to be due to the combination of a relatively thick ($\sim$1 μm) surface layer having low lifetime. The low lifetime results from the high doping levels which were used to achieve the abrupt junctions. The use of a thinner epitaxial surface layer could not be explored because the reproducible growth of submicron layers could not be achieved with the present epitaxial techniques. However, an examination of the data does reveal a trend toward higher short-circuit current for those samples with thinner surface layers (see table 4).

In the next section, we describe several methods which can be used to obtain better blue response and correspondingly higher short-circuit current density.

C. Short-Circuit Current – Cell Efficiency

1. Comparison of Epitaxial and Diffused Surface Layers

Since submicron surface layers could not be grown, two alternate approached were explored. The first of these was simply to grow the base layer and subsequently diffuse a shallow junction into it. For
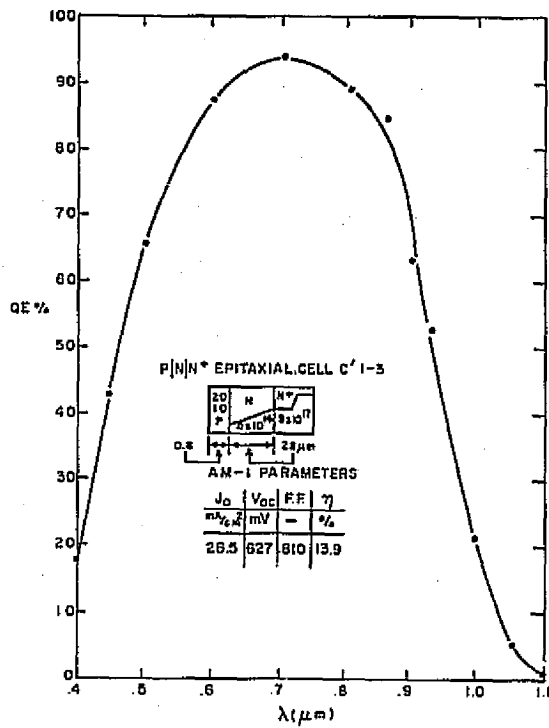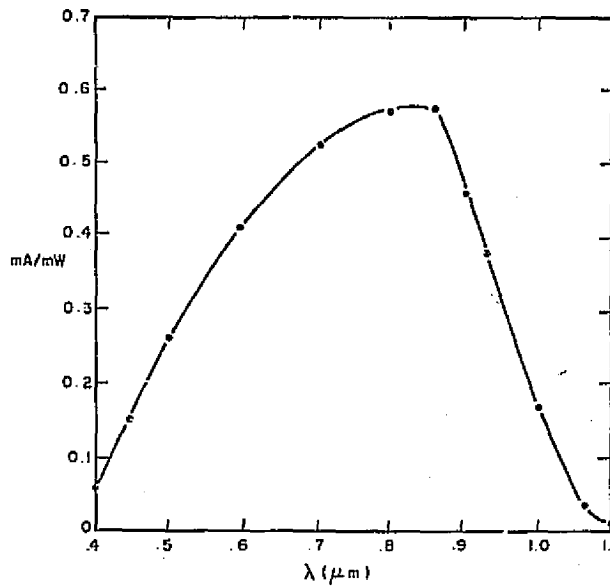
Figure 20. (a) Spectral response for p/n/n⁺ epitaxial solar
cell C'1-3.
(b) Spectral response (mA/mW) for same sample as
(a).

the case of n-base layers, we formed the $p^+/n/n^+$ structure using a boron deposition and diffusion technique (ref. 15) which has proven to be effective in forming high-efficiency cells in bulk n-type silicon wafers. The second approach consisted of growing a surface layer of about 1-μm thickness having a lower dopant concentration ($\leq 5 \times 10^{18}$ A cm^{-3}) than in our previous all-epitaxial structures, and then diffusing a shallow (~ 0.2 μm) region into the surface. The diffusion is done primarily to lower the surface-layer sheet resistance, and if done properly, it can also provide a "built-in" electric field which aids in reducing the effect of surface recombination.

Solar-cell performance and spectral responses which are typical of those obtained using the two methods described above are shown in figure 21. In both cases substantial improvement in blue response and higher short-circuit current density was obtained, with the largest gain (+12%) in short-circuit current density obtained for the samples having a shallow diffused surface layer.

It should be noted that the fill-factor and open-circuit voltage are lowest in the case of shallow diffused surface layers. We have found this to occur in general for such structures.

2. Solar-Cell Results – $n/p/p^+$ Structures

A more detailed study of diffused and epitaxial surface layers was conducted for $n/p/p^+$ structures. In this case a three-way matrix was run in which the p-base layer profile was held fixed (~ 60 μm graded from 1×10^{16} to 1×10^{17} A cm^{-3}) and three different n-type top layers were constructed. Groups I and III were fabricated by growing an n-type (arsenic doping) top layer with a light doping concentration of $\sim 5 \times 10^{17}$ A cm^{-3} (0.05 Ω-cm) followed by a shallow (<0.2 μm) n$^+$ phosphorus diffusion at 900°C in a separate furnace. The surface-layer thickness for group III structures was intentionally made approximately six times (3 μm vs 0.5 μm) greater than that for group I samples. For group II structures, the n$^+$ diffusion was applied directly to the as-grown p-base layers.
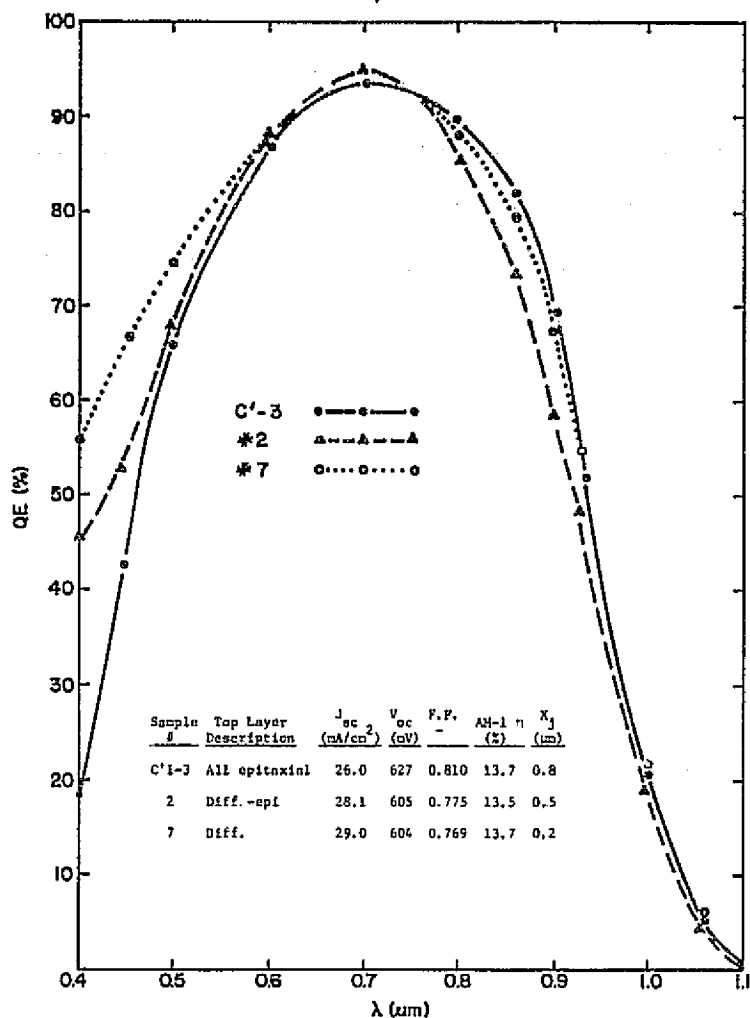
Figure 21. Spectral response and tabular summary for p/n/n$^+$ solar cells having different p- layer structures.

Sample #	Top Layer Description	J_{sc} (mA/cm^2)	V_{oc} (mV)	F.F.	AM-1 η (%)	X_j (μm)
C'1-3	All epitaxial	26.0	627	0.810	13.7	0.8
2	Diff.-epi	28.1	605	0.775	13.5	0.5
7	Diff.	29.0	604	0.769	13.7	0.2

The details of the profiles along with the measured AM-1 illuminated cell parameters for the three groups are given in table 6. The samples labeled FZ were fabricated in bulk float-zone crystals as controls for the diffusion process. Spectral response curves typical of each group and one of the controls are shown in figures 22, 23, 24, and 25.

It is interesting to note that the short-circuit current densities obtained with group III structures are quite comparable to the others

TABLE 6. SUMMARY OF GROUPS I-III – PROFILES AND AM-1 ILLUMINATED PARAMETERS

Group Sample	Surface Layer n-Top Layer Description	x_j (μm)	R * ($\Omega/\square$)	Base Thickness (μm)	p-Base Layer Profile	NA (A cm^{-3})	J_{sc} (mA/cm^2)	V_{oc} (mV)	F.F. —	η (%)
Group I										
155221	Diff. + Epi	0.3	1060/230	58	Graded	$1 \times 10^{16}/$ 1×10^{17}	30.8	575	0.781	14.1
155081	Diff + Epi	0.2	1550/180	69	Graded	$1.5 \times 10^{16}/$ 1×10^{17}	30.0	574	0.780	13.7
I – FZ	Diffused	0.2	320	300	Bulk 1.5Ω-cm	1×10^{16}	31.0	570	0.745	13.6
Group II										
154901	Diffused	0.2	258	75	Graded	$1.5 \times 10^{16}/$ 1×10^{17}	30.8	562	0.630	11.1
155001	Diffused	0.2	390	59	Graded	$1 \times 10^{16}/$ 1×10^{17}	29.5	556	0.627	10.5
II – FZ	Diffused	0.2	151	300	Bulk 1.5Ω-cm	1×10^{16}	28.5	555	0.625	10.1
Group III										
155508	Diff. + Epi	2.0	510/189	51	Graded	$1 \times 10^{16}/$ 1×10^{17}	29.8	570	0.807	14.0
155348	Diff. + Epi	3.0	280/240	69	Graded	$2 \times 10^{16}/$ 1×10^{17}	29.0	576	0.676	11.6
III – FZ	Diffused	0.2	137	300	Bulk 1.5Ω-cm	1×10^{16}	30.0	585	0.717	12.9

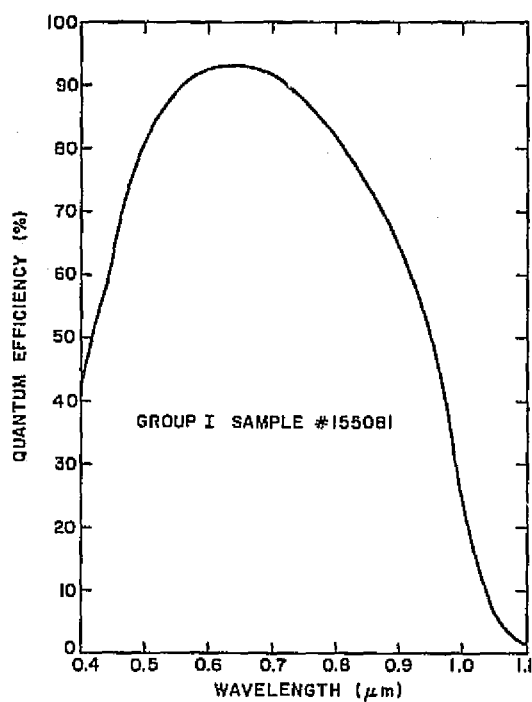*The two values of R given are before/after the n$^+$ diffusion.

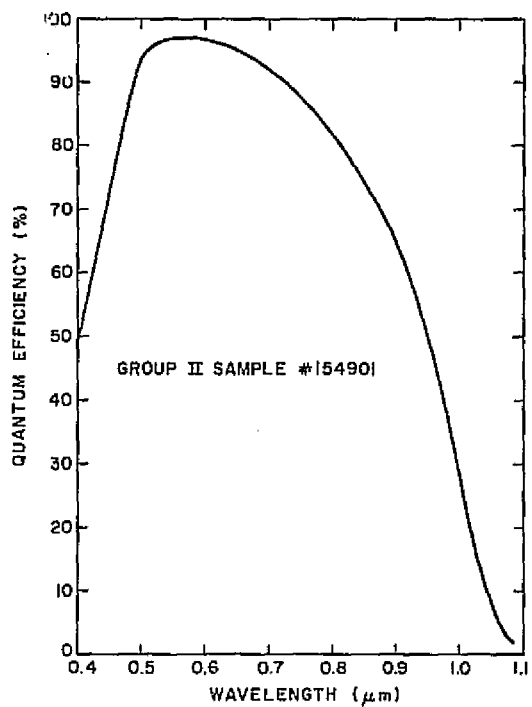Figure 22. Spectral response curve for group I sample 155081.

Figure 23. Spectral response curve for group II sample 154901.

38
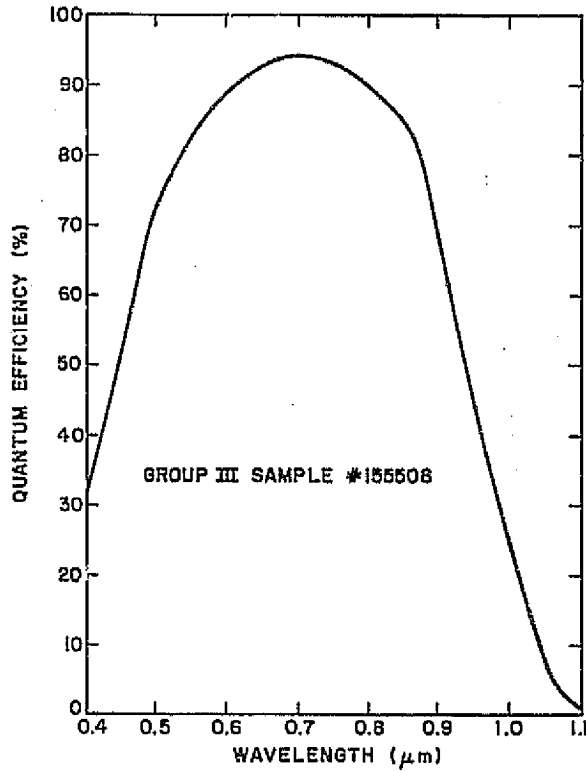
Figure 24.   Spectral response curve for group III sample 155508.
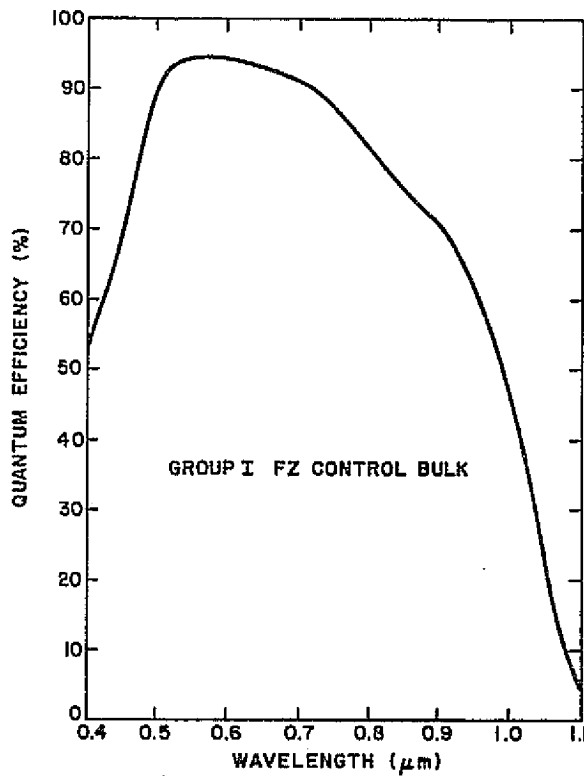
Figure 25.   Spectral response curve for group I control bulk sample.

even though the junction depths for group III cells are 2 to 3 μm. This is most likely due to the lower doping concentration used in the growth of these surface layers which should result in longer diffusion lengths than those in the more highly doped 1-μm-thick surface layers previously studied.

The major conclusion that can be drawn from these data is that AM-1 short-circuit current densities of $\sim$30 mA/cm^2 (this corresponds to an AM-0 value of $\sim$36 mA/cm^2) and AM-1 efficiencies of 14% can be obtained with 50-μm-thick epitaxial cells provided that special attention is paid to the properties of the surface layer so as to achieve good blue response.

SECTION IV

CONCLUSIONS

Listed below are the major conclusions drawn from the work conducted under this contract in which studies were made of both variations in base-layer and surface-layer profiles in epitaxial structures.

(1) For those structures which would potentially yield the highest cell characteristics, it is difficult to separate the base-layer and surface-layer contribution to cell performance.

(2) When the surface layer is grown in such a manner as to obtain an abrupt junction characteristic on a 25- to 50-μm-thick base layer having a doping level $\gtrsim 5 \times 10^{16}$ A cm^{-3}, reproducible open-circuit voltages of ∿625 mV were obtained. The AM-1 efficiency of such structures is limited to ∿13% primarily by values of short-circuit current density $\lesssim$25 mA/cm^2. This condition is related to limitations in the present surface-layer growth techniques which result in 1-μm-thick layers having relatively short diffusion length.

(3) The epitaxial junctions yield near-ideal electrical junction characteristics which result in fill-factors generally $\gtrsim 0.80$.

(4) By examination of base layers in the 25- to 50-μm thickness range, with a variety of exponential doping gradients we conclude that such gradients are beneficial in enhancing short-circuit current density in structures having diffusion lengths less than the base thickness.

From our studies of surface layers several conclusions can be drawn concerning the necessary growth conditions and properties of

such layers for the attainment of high V_{oc} and cell efficiency. These are:

(1) Abrupt junctions must be obtained by careful attention to the epitaxial growth conditions (i.e., temperature, dopant concentration, flush cycles, and gas flow) used in forming the surface layer.

(2) Such abrupt junctions can be obtained by limiting diffusion process during epi growth by lowering the temperature, decreasing the time and increasing the doping level during and after the growth of the surface layer.

(3) High doping concentrations ($\geq 10^{20}$ A cm^{-3}) in surface layers ≥ 1 µm in thickness result in solar cells with $J_{sc} \leq 25$ mA/cm^2 because of poor blue response.

(4) Increased blue response with a corresponding increase in short-circuit current density to ~ 30 mA/cm^2 can be achieved with a surface layer formed by a combination of epitaxial growth with a lower concentration ($\geq 1 \times 10^{18}$), and the subsequent diffusion of a thin highly doped region into this surface. Similar short-circuit currents were achieved with surface layers formed by direct diffusion of a shallow junction into the base layer. However it was found that in such cells, the fill-factor and open-circuit voltage were lower than in the all-epitaxial structures.

Although no experimental studies of the radiation resistance of these epitaxial cells were conducted at RCA, several samples supplied to NASA-Lewis showed good performance up to the radiation levels normally encountered in space applications.

SECTION V

RECOMMENDATIONS

High open-circuit voltage and very good fill-factors were repro-
ducibly obtained with the epitaxial techniques and structures reported
here. The major ingredients necessary for achieving efficiencies
higher than 14% (AM-1) are the attainment of higher short-circuit cur-
rent density and even higher open-circuit voltage. Our work has pin-
pointed a number of areas where improvements and further research and
development are required in order to realize the full potential of the
epitaxial method. These form the basis of the following recommenda-
tions.

Surface Layers

Since the properties of the surface layer play an important but
poorly understood role in determining cell performance, we recommend
a more detailed and comprehensive study of surface layers. Several
specific areas needing further work are:

(1) Development of techniques for the reproducible growth of
surface layers of thickness less than 0.5 µm, simultaneous
with the ability to control the doping profile.

(2) A better theoretical understanding and the development of
simplified models describing the role of surface layers
in cell performance.

(3) Additional methods should be developed for the study of
doping profiles, both of total and electrically active
dopant concentrations, in order to provide more information
on the level of concentration at which cell performance
begins to degrade. The SIMS technique used in the work
reported here is very well suited for the study of total
dopant concentration and profile. The development and
use of spreading resistance techniques for submicron layers

43

would provide a useful method for the measurement of electrically active profiles. Combined studies by the SIMS and spreading resistance techniques would be useful in relating the profile shapes to solar-cell performance.

(4) Methods for the attainment of longer diffusion lengths, especially at higher doping concentrations ($>10^{18}$ A cm^{-3}) should be pursued.

Base Layers

Further studies are needed of base layers having doping concentrations in excess of 10^{17} A cm^{-3}. Specifically, we recommend a study of the role of concentration level, impurity incorporation, and defect density in limiting the diffusion length. The attainment of longer diffusion lengths in the structures we have fabricated would result in increases in open-circuit voltage above 625 mV and an increase in short-circuit current.

Radiation Resistance

The radiation resistance properties of thin epitaxial solar cells should be more fully evaluated.

44

REFERENCES

1. R. V. D'Aiello, P. H. Robinson, and H. Kressel, *Epitaxial Solar Cell Fabrication*, Final Report prepared for Nasa-Lewis Research Center under Contract NAS3-19401, Dec. 1975.

2. R. V. D'Aiello, P. H. Robinson, and H. Kressel, Appl. Phys. Letters 28, 231 (1976).

3. S. M. Sze and J. C. Irvin, Solid State Electronics 11, 599 (1968).

4. J. Mandelkorn and John H. Lamneck, Jr., Conference Record, Ninth IEEE Photovoltaic Specialists Conference, Silver Spring, MD, 1972, p. 66.

5. H. W. Brandhorst, Jr., C. R. Baraona, and C. K. Swartz, Conference Record, Tenth IEEE Photovoltaic Specialists Conference, Palo Alto, CA, 1973, p. 212.

6. J. Lindmayer, *"Development of 20% Efficient Solar Cell*, Final Report, NSF Grant GI-43090, Oct. 1975, p. 87.

7. M. P. Godlewski, C. R. Baraona, and H. W. Brandhorst, Jr., Conference Record, Tenth IEEE Photovoltaic Specialists Conference, Palo Alto, CA, 1973, p. 40.

8. J. Mendelkorn and J. H. Lamneck, Conference Record, Eleventh IEEE Photovoltaic Specialists Conference, Scottsdale, AZ, 1975, p. 36.

9. J. W. Slotboom and H. C. De Graaff, Solid State Electronics 19, 857 (1976).

10. J. W. Slotboom, Solid State Electronics 20, 279 (1977).

11. M. P. Godlewski, H. W. Brandhorst, Jr., and C. R. Baraona, Conference Record, Eleventh IEEE Photovoltaic Specialists Conference, Scottsdale, AZ, 1975, p. 32.

12. F. A. Lindholm, S. S. Li, and C. T. Sah, Conference Record, Eleventh IEEE Photovoltaic Specialists Conference, Scottsdale, AZ, 1975, p. 3.

13. P. M. Dunbar and J. R. Hanser, Conference Record, Eleventh IEEE Photovoltaic Specialists Conference, Scottsdale, AZ, 1975, p. 13.

14. C. R. Baraona and H. W. Brandhorst, Jr., Conference Record, Twelfth IEEE Photovoltaic Specialists Conference, Baton Rouge, LA, 1976, p. 6. Also C. R. Baraona and C. K. Swartz, private communication.

15. M. S. Bae and R. V. D'Aiello, Appl. Phys. Letters 31, 285 (1977).

16. H. J. Hovel, *Semiconductors and Semimetals*, vol. 2, "Solar Cells," (Academic Press, New York, 1975) p. 41.

APPENDICES

APPENDIX A

SECONDARY ION MASS SPECTROMETER (SIMS)

One of the primary tools used for analyzing the impurity profiles obtained by the growth of shallow junction surface layers described in Section III.B of the main body of this report is the secondary ion mass spectrometer (SIMS). Based on extensive experience with the CAMECA ion microscope, we have designed and built an instrument of comparable sensitivity and depth resolution, with several added features which enhance the accuracy and ease of depth profiling.

The system built at RCA Laboratories is a secondary ion quadrapole mass spectrometer. Figure A-1 shows some of the overall features of this instrument. The entire instrument is made from UHV components. The primary ion gun is differentially pumped with a 1200-ℓ/s diffusion pump and the target chamber is pumped with a 220-ℓ/s ion pump and a titanium sublimation pump with a large ℓN_2 cold wall. The latter two are especially useful when employing an oxygen jet directed at the sample to increase positive secondary ion yields. C_s primary ion bombardment is used to increase negative ion yields. Up to eight samples are mounted on a high precision sample manipulator and are viewed during analysis with a 30X stereo microscope with coaxial illumination normal to the sample surface. Another very important feature of this instrument is automated instrument control and data collection for multi-element depth profiles. We use a Hewlett-Packard programmable calculator[*] (Model #9830A) to monitor up to six masses with the quadrapole, read the accumulated ion counts from a counter after a preset dwell time on each mass, and process the data at the end of the run and plot the profiles. This is an area where the quadrapole mass spectrometer has an unparalleled advantage over the magnetic sector instrument. Our machine can change 100 amu in less than 10 ms and reproduce peak position to within 0.01 amu with drift of <0.01 amu/h. The speed and reproducibility of the quadrapole allow data to be taken directly on the peak top (no need to
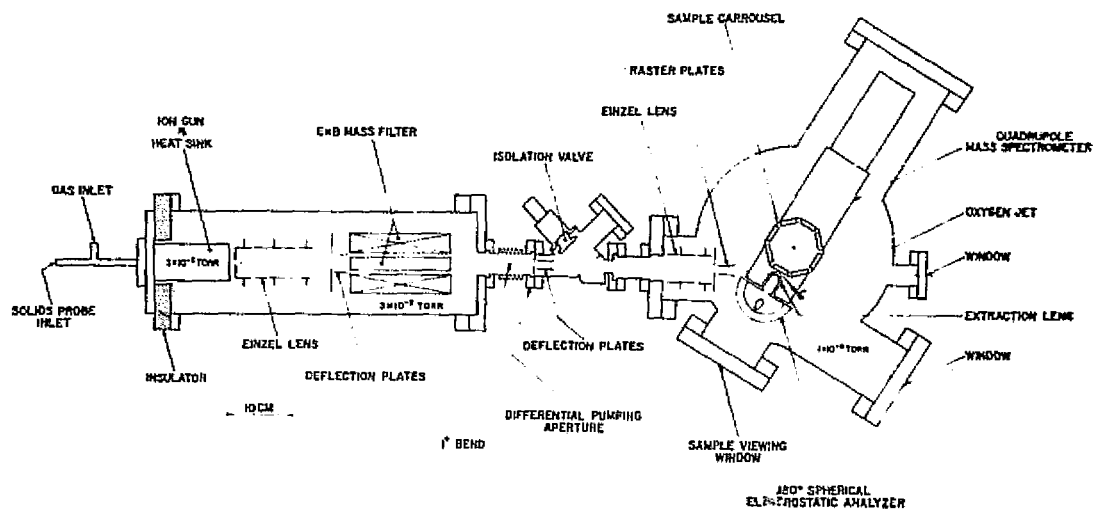
[*]Hewlett-Packard Corp., Palo Alto, CA.

Figure A-1. SIMS (Quadrapole) machine constructed at RCA Laboratories.

scan over the peak) and, if necessary, all six elements can be measured in less than 1 s.

Figure A-2 shows how our SIMS instrument has sensitivity and depth resolution comparable to those of the commercially available ion micro-analyzers. The figure also demonstrates the abundance sensitivity of our instrument, or the ability to measure a very small peak immediately adjacent to a large peak. This profile was taken by monitoring the Al + peak at mass 27, 1 amu away from the 92% isotope of silicon at mass 28. The aluminum was followed to a level of 0.2 ppma. Note also the sputtering rate for the analysis of 7.6 Å/s. Shallow (<0.2 µm) diffused boron profiles have also been measured with similar resolution and sensitivity. An ion-implanted and annealed profile of ^{11}B is shown in figure A-3. Agreement with the calculated profile is used for boron calibration. Presently, measurements and calibrations are being made for arsenic and phosphorus profiles in silicon; however, these were not available during the period of the contract.
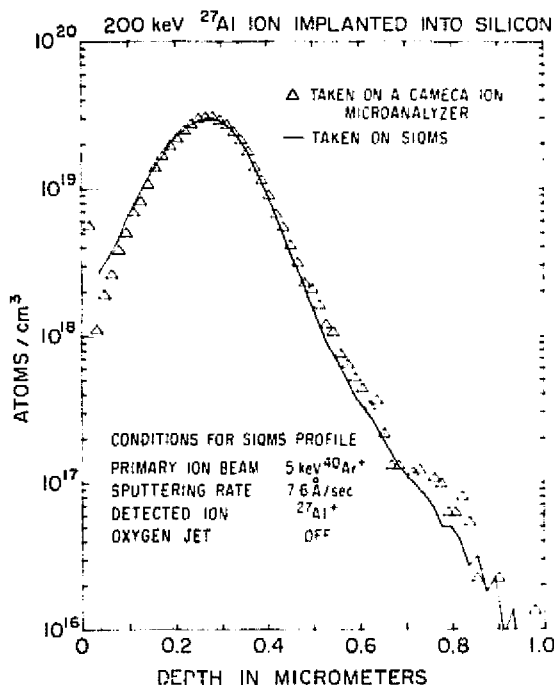
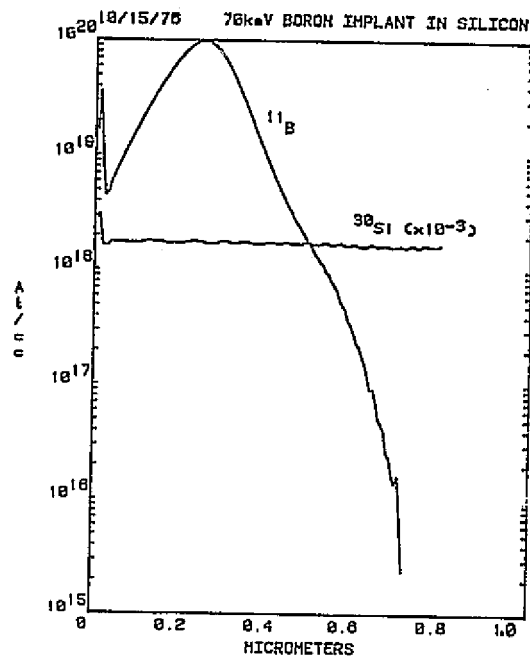Figure A-2. Measured profile of 200-keV ^{27}Al ion implanted into silicon.

Figure A-3.   Measured profile of 70-keV boron implanted
into silicon.

APPENDIX B

COMPLETE MEASURED PROFILE OF p/n/n^{++} SOLAR CELL
WHICH HAS THE HIGHEST OPEN-CIRCUIT VOLTAGE

After the surface-layer profiling technique (SIMS) described in Appendix A was developed and applied with success to several solar-cell structures, we decided to section the solar cell which had the highest open-circuit voltage (636 mV) voltage. The detailed performance of this cell was reported in the final report describing our first year's work (ref. 1) and in the literature (ref. 2). A copy of reference 2 is included here for reference. The cell described here is the one referred to as structure I in that publication.

This cell is a p^{+}/p/n/n^{++} structure, having an epitaxially grown n-base layer and a diffused/epitaxial surface p^{+}/p-layer. The surface-layer profile was measured using SIMS; the base-layer profile near the
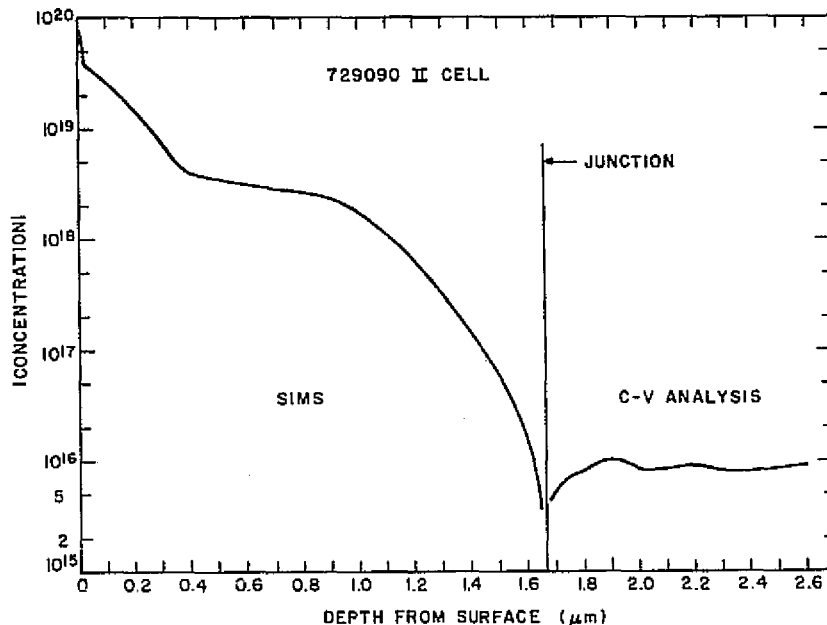

Figure B-1. Surface-layer profile for sample 729090 as determined by SIMS and a portion of the base-layer profile as determined from C-V analysis.

junction was determined by C-V analysis, and a complete base-layer profile was measured by spreading resistance. The surface-layer boron concentration profile and near-junction base profile are shown in figure B-1. The complete base-layer profile is given in figure B-2.
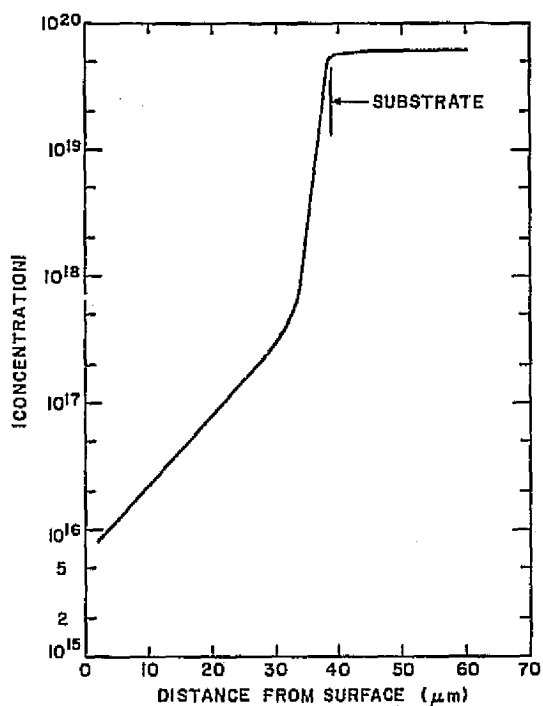

Figure B-2. Base-layer profile for sample 729090 is determined from spreading resistance analysis.
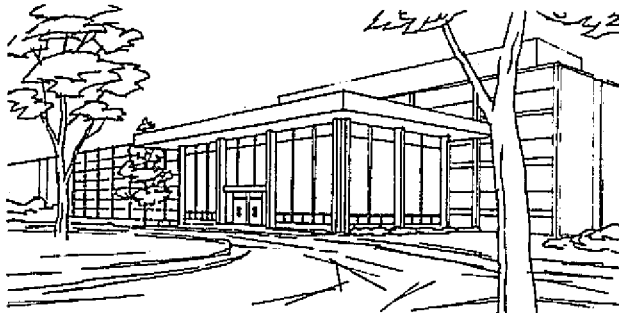
Epitaxial Silicon Solar Cells

R. V. D'Aiello, P. H. Robinson and H. Kressel

RCA LABORATORIES   PRINCETON, NEW JERSEY

DAVID   SARNOFF   RESEARCH   CENTER

Epitaxial silicon solar cells*

R. V. D'Aiello, P. H. Robinson, and H. Kressel

RCA Laboratories, Princeton, New Jersey 08540
(Received 10 October 1975)

$p^+/p/n/n^+$ epitaxial silicon solar-cell structures were fabricated with the n-base region intentionally graded over 2 orders of magnitude in a thickness of 35 μm. Solar cells made from these layers exhibited near-ideal I-V characteristics in the practical operating range, with an open-circuit voltage of 636 mV, fill factor of 0.79, and AM1 efficiency of 12.6%. A similar epitaxial structure containing no gradient in the n-base showed good solar-cell performance but lower open-circuit voltage (603 mV).

Extensive effort has been devoted towards the development of efficient silicon solar cells using diffusion technology.[1-3] Although improvements in efficiency have been obtained,[2] a major limitation of the present diffused cells is in obtaining near-ideal current-voltage (I-V) characteristics for the shallow junction and high doping concentrations required for high open-circuit voltage and efficient solar-cell operations.[4,5] Recently, an epitaxial technology for the fabrication of silicon

solar cells has been proposed[6] which appears to reduce this difficulty while offering flexibility of structural design. This letter reports preliminary results on the fabrication and operating characteristics of relatively thin $p^+/p/n/n^+$ epitaxial silicon solar cells (~40 μm thick) containing intentional doping gradients in the n-base layer. One such cell having an exponential doping grade has a measured power conversion efficiency (AM1) of 12.6% with a fill factor of 0.79 and open-cir-
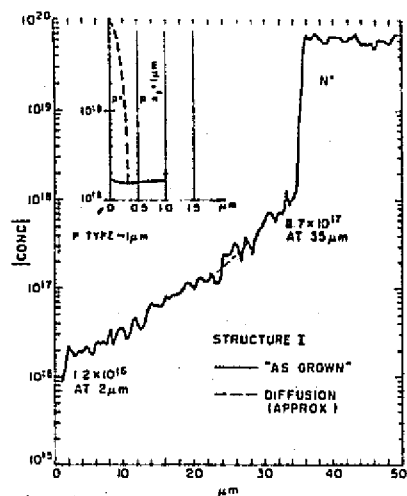
(a)
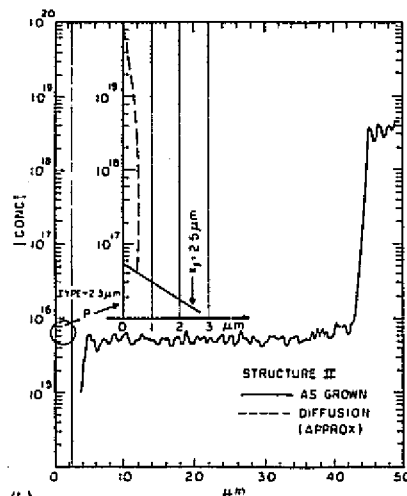
(b)

FIG. 1. Doping profiles determined by two-point spreading resistance for the two $p^+/p/n/n^+$ structures. (a) Graded n-base, structure I; (b) uniform n-base, structure II.
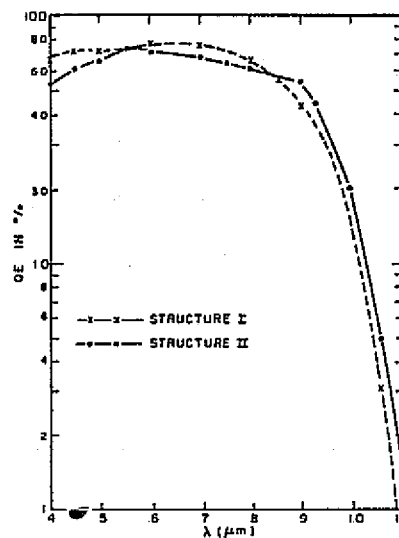

FIG. 2. Spectral response vs wavelength.

formed by standard photolithography. The edges of the cell and diodes were mesa etched to a depth of 2 mils. Finally, an AR coating of 700 Å of Al_2O_3 was evaporated over the cell structures.

The resulting doping profiles for the two solar-cell structures reported here, as obtained from spreading resistance measurements, are shown in Figs. 1(a) and 1(b). In the insets of these figures, the dashed curves representing the p^+ diffusions are only approximate, as
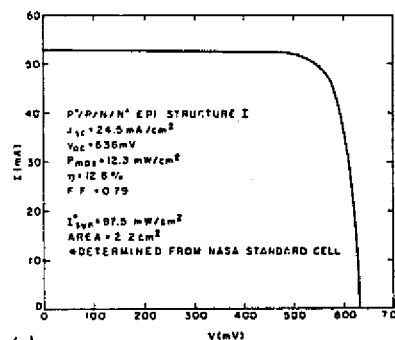
(a)
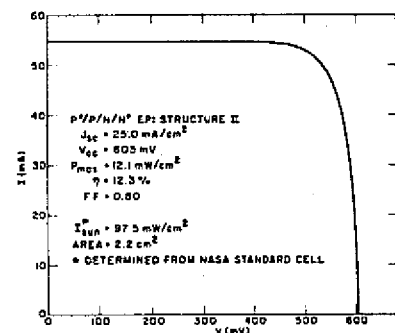
(b)

FIG. 3. Output I-V curves measured in sunlight at an incident radiation intensity of 97.5 mW/cm^2 for (a) structure I and (b) II structure.

cuit voltage of 636 mV, the highest open-circuit voltage reported to date. These results are compared to a cell having a similar structure but with a uniform doping profile in the n-base region.

The epitaxial n and p layers were grown in a horizontal reactor using dichlorosilane[7] as the silicon source material. The doping gases were arsine and diborane diluted with purified hydrogen. All layers were grown at 1100 °C at a growth rate of 5 μm/min on $\langle 111 \rangle$-oriented n^+ substrates.

After removal from the epitaxial reactor, a p^+ region was diffused approximately 0.3 μm into the top p layer in a separate furnace at 925 °C using a boron-doped silane deposited oxide. The wafers are then stripped of all oxides and metallized by evaporation of Cr/Au for the top contact and Cr/Ni on the back. The solar-cell structure containing 11 fingers (15% metal coverage) with a total area of 2.2 cm^2 along with six diagnostic diodes in close proximity to the solar cell was then

54

TABLE I. Summary of solar cell and diode parameters. Cell area, 2.18 cm².

Solar-cell structure		J_{sc}[a] (mA/cm²)	V_{oc} (mV)	P_{max} (mW/cm²)	η (%)	Fill factor	J_0[b] (A/cm²)	n[b]	J_0[c] (A/cm²)	n[c]	τ_n[d] (μs)
I	$p^+/p/{}^{graded}_{n}/n^+$	24.5	636	12.3	12.6	0.79	9×10^{-13}	1.03	1.8×10^{-12}	1.04	1.5
II	$p^+/p/{}^{uniform}_{n}/n^+$	25.0	603	12.1	12.3	0.80	5.4×10^{-12}	1.05	5×10^{-12}	1.07	3.6

[a]Measured at incident solar intensity of 97.5 mW/cm².
[b]Obtained from $V_{oc} = (nkT/q) \ln[(J_{sc}/J_0)+1]$ (Fig. 4).
[c]Obtained from I-V curves of diodes.
[d]Average value as measured by reverse recovery and open cir-cuit decay techniques.

the spreading resistance profiles are subject to great errors for very shallow diffusions.[8] The doping gradi-ent in the n-base layer of structure I was intentionally introduced in order to produce a drift field for enhanced collection of the photogenerated minority carriers.

Spectral response curves and illuminated I-V charac-teristics of the solar cells were measured using an AM1 solar simulator lamp at incident radiation intensity of 100 mW/cm². Solar-cell performance was also mea-sured under New Jersey sunlight conditions. In all cases, the radiation intensity was measured using calibrated solar cells provided by NASA.[9] Dark I-V characteristics and minority-carrier lifetimes were measured on the adjacent diodes by the reverse recovery and open-cir-cuit—voltage decay method.

Figures 2(a) and 2(b) show the spectral response curves and Figs. 3(a) and 3(b) show the sunlight operat-ing I-V characteristics for the two solar-cell structures of Fig. 1. Table I summarizes the pertinent solar-cell and diode parameters. The parameters J_0 and n related to the I-V characteristics $J(V) = J_0 \exp[(qV/nkT)-1]$ were also determined from a measurement of J_{sc} vs V_{oc} for various incident radiation intensities,[10] as shown in Fig. 4.

The high fill-factor and open-circuit voltage result, for the most part, from the near-ideal I-V character-

istic of the grown epitaxial p-n junctions. This is seen, for example, in the case of structure I (Fig. 4) by the n factor of 1.03 and saturation current density J_0 of 9×10^{-13} A/cm² in the diffusion-dominated portion of the I-V characteristic, which extends from ~560 mV to beyond the open-circuit voltage. This was achieved by having a relatively low doping level in the immediate vicinity of the grown p-n junction (thus minimizing dop-ing-related defects). Such defects contributed to the nonideal I-V characteristics of shallow diffused junc-tions with high surface concentrations of the kind typi-cally used for solar-cell fabrication.[11]

It is interesting to compare our measured saturation current density values to those calculated assuming ideal conditions (i.e., the diffusion-limited case) and ignoring the effects of both the doping gradient and the n/n^+ junction.[12] J_0 is then given by

$$J_0 = q n_i^2 \left[\frac{1}{N_D} \left(\frac{D_p}{\tau_p} \right)^{1/2} + \frac{1}{N_A} \left(\frac{D_n}{\tau_n} \right)^{1/2} \right], \tag{1}$$

For structure II, using $\tau_p = 3.6$ μs, $\tau_n = 0.5$ μs, $D_p = 10$ cm²/sec, and $D_n = 8$ cm²/sec, the calculated $J_0 = 4.8 \times 10^{-12}$ A/cm², in excellent agreement with the measured value of 5.4×10^{-12} A/cm².

For the graded-base structure I, the theoretical value calculated as above except with $\tau_p = 1.5$ μs is $J_0 = 4.7 \times 10^{-12}$ A/cm². This value is ~5 times higher than the measured one, a discrepancy we attribute to ignoring the field-gradient terms which tend to reduce the saturation current density. These calculations indi-cate that the reduction in J_0 and the consequent increase in open-circuit voltage for structure I result from the effect of the doping gradient in the n-base layer. En-hanced solar-cell performance due to doping gradients in the base layer was theoretically predicted by Ellis and Moss.[13]

The moderately high efficiency obtained with the pres-ent structure results from the large open-circuit voltage and good fill factor, while the short-circuit current is below that normally obtained in high-efficiency cells. However, since the present base-layer thickness is less than a diffusion length, thicker layers with graded pro-files should result in a higher short-circuit current, and thus higher efficiency.

In conclusion, 12.6% efficient silicon solar cells with near-ideal I-V characteristics, high open voltage, and fill factor were obtained with epitaxially grown $p^+/p/n/n^+$ structures. The epitaxial technique was used to com-pare similar structures having uniform and intentionally
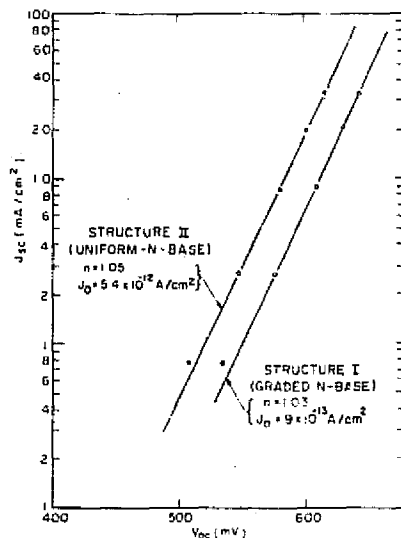

FIG. 4. Determination of junction parameters n and J_0 for structures I and II.

graded n-base layers. It was found that the graded structure yielded a substantially higher open-circuit voltage (636 mV vs 603 mV) than a structure with uniform doping with no appreciable degradation in other cell parameters. Thus, the flexibility and control afforded by the epitaxial approach to high-efficiency silicon solar cells allows for simultaneously obtaining high open-circuit voltage and good-quality junctions.

The authors would like to thank D.R. Patterson for technical assistance with the optical and electrical measurements; J. Murr, D. Tarangioli, J. Jaklik, and W. Wance for various aspects of fabrication and measurement. We also appreciate discussions and reading of the manuscript by D. Redfield.

[1]P. Rappaport and J.J. Wysocki, *Photoelectronic Materials and Devices*, edited by S. | ~ach (Van Nostrand, New York, 1965).
[2]J. Lindmayer and J. Allison, *Proceedings of the 9th IEEE Photovoltaic Conference, Silver Spring, Maryland, 1972* (IEEE, New York, 1972), p. 83.
[3]M. Wolf, J. Energy Conversion 11, 63 (1971).
[4]M.P. Godlewski, H.W. Brandhorst, and C.R. Baraona, *Proceedings of the 11th IEEE Photovoltaic Specialists Conference, Phoenix, 1975* (IEEE, New York, 1975), p. 32.
[5]M. Wolf, *Proceedings of the 10th IEEE Photovoltaic Specialists Conference, 1973* (IEEE, New York, 1973), p. 5.
[6]V.L. Dalal, H. Kressel, and P.H. Robinson, J. Appl. Phys. 46, 1283 (1975). The use of single epitaxial layers in connection with radiation damage resistance was suggested by J. Mandelkorn, *et al.*, in Ref. 5, pp. 207—211 and by H. Brandhorst *et al.*, in Ref. 5, pp. 212—217.
[7]N. Goldsmith and P.H. Robinson, RCA Rev. 34, 358 (1973).
[8]N. Goldsmith, R.V. D'Aiello, and R.A. Sunshine, *Proc. Spreading Resistance Symposium, 1974, Nat'l. Bur. Stds. Special Publication No. 400-10 (1974)* (U.S. GPO, Washington, D.C., 1974), pp. 223—234.
[9]C. Swartz and H.W. Brandhorst (private communication).
[10]M. Wolf and H. Rauschenbach, Adv. Energy Conversion 3, 455 (1963).
[11]F.A. Lindholm, S.S. Li, and C.T. Sah, in Ref. 4, pp. 3—12.
[12]M.P. Godlewski, C.R. Baraona, and H.W. Brandhorst, in Ref. 5, pp. 40—47.
[13]B. Ellis and T.S. Moss, Solid-State Electron. 13, 1 (1970).

APPENDIX C

SURFACE-LAYER ETCHING EXPERIMENT

An experiment was conducted in an attempt to relate the short-circuit current to the thickness of the top layer in a $p^+p/n/n^+$ epitaxial solar cell. The experiment consisted of etching away the p^+p-surface layer in approximately 0.15-μm steps with an illuminated I-V measurement taken between etch step. The use of a KOH etchant solution at 80°C allowed for the slow etching of silicon without seriously degrading the Ti/Ag metallization.

The SIMS profile of the p^+p layer measured on a section of the wafer adjacent to the cell is shown in figure C-1 and the epitaxial n-base profile is shown in the inset. The p^+ region of ~0.3-μm depth was obtained by diffusion from a boron-doped oxide source at 950°C after the structure was epitaxially grown.
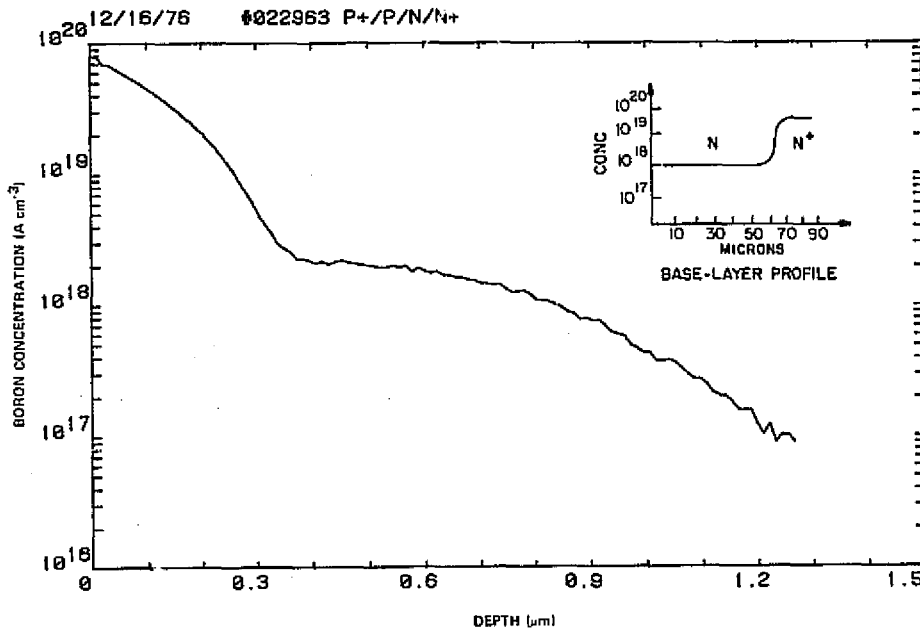

Figure C-1. SIMS concentration profile for boron in the top layer of $p^+p/n/n^+$ solar-cell structures used in the etching experiment. Base-layer profile shown in the inset.

The results of nine etch steps and I-V measurements are shown in figure C-2. The first measurement (zeroth step) was done with the AR coating intact; after removal of the AR coating, a second measurement (not shown in figure C-2) was made and a 1.42 ratio of short-circuit current before and after AR coating removal was used to correct all subsequent data.
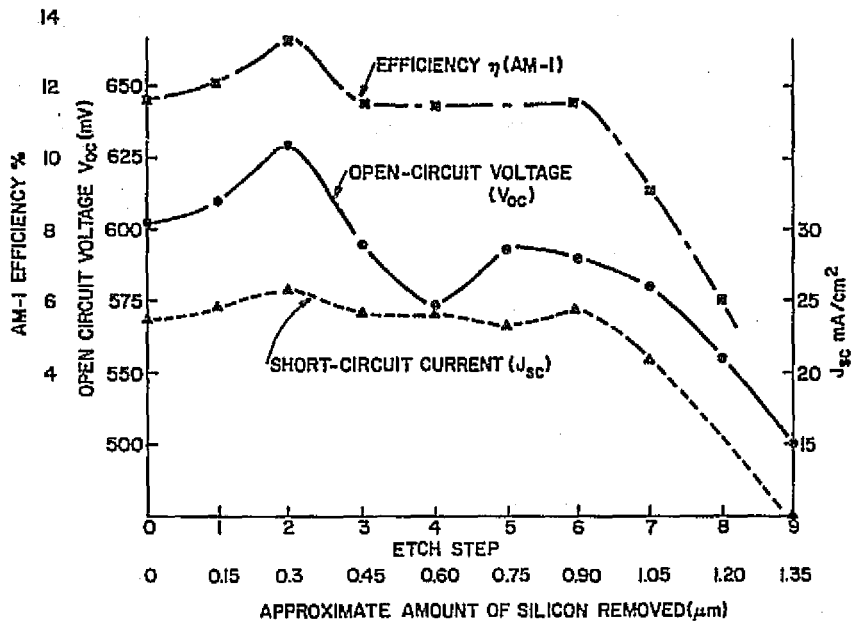

Figure C-2.   AM-1 efficiency, open-circuit voltage, and short-circuit current as a function of silicon removal from the top layer.

The data are surprising in two respects. The large increase in open-circuit voltage of ~25 mV with the removal of ~0.2 to 0.3 µm from the top layer was unexpected. Second, the short-circuit current increased at first ~9% and then remained relatively unchanged until almost the entire top layer was removed. The increase in short-circuit current at the first and second etch steps could be related to a slight "texturizing" of the front surface caused by the KOH etch. The subsequent constancy of J_{sc} with decreasing front-layer thickness is puzzling since

it was expected that as the front layer became very thin, the short-circuit current would increase. One model (ref. 16) which qualitatively fits these data is that of a top layer with low surface recombination velocity, no drift field, and no dead layer. After removal of the first 0.3 μm, the profile shown in figure C-1 is consistent with this model.

The increase in open-circuit voltage of $\sim$25 mV with the removal of the first 0.3 μm corresponds to a decrease in saturation current density by about a factor of three. This means that the dark current for this structure is dominated by the contribution from the top layer and in particular from the diffused 0.3-μm portion. Since the base layer in this structure is doped at $\sim$10^{18} A cm^{-3}, the dark-current contribution from the base layer is very small and the results obtained show the control of open-circuit voltage exerted by the properties of the top layer in such structures.

APPENDIX D

SOLAR CELLS MEASURED AT NASA-LEWIS AND RCA

Seven epitaxial solar cells representative of those reported here
were sent to the NASA-Lewis Measurements Laboratory for verification
of performance. Table D-1 gives a summary of the AM-1 parameters
measured at NASA-Lewis and at RCA, and figures D-1 through D-7 show
the illuminated AM-0 I-V characteristics and parameters measured at
NASA.

TABLE D-1. SUMMARY OF ILLUMINATED CELL MEASUREMENTS CONDUCTED AT NASA–LEWIS AND RCA

	NASA AM-1 SIMULATION @ 28°C				RCA LABS AM-1 SIMULATION				RCA LABS OUTDOORS			
Cell No.	J_{sc} (mA/cm^2)	V_{oc} (mV)	F.F. –	η (%)	J_{sc} (mA/cm^2)	V_{oc} (mV)	F.F. –	η (%)	J_{sc} (mA/cm^2)	V_{oc} (mV)	F.F. –	η (%)
C-1	24.3	616	0.814	12.6	25.8	620	0.810	13.0	25.0	623	0.811	13.0
C-2	20.0	603	0.788	9.8	21.4	610	0.770	10.3	20.5	605	0.799	10.0
C-3	22.1	616	0.804	11.4	23.4	618	0.802	11.9	22.7	620	0.820	12.0
C-A	21.5	618	0.803	11.0	22.7	625	0.806	11.8	22.3	620	0.813	11.7
C-B	23.5	608	0.798	11.8	25.6	620	0.770	12.5	24.6	615	0.815	12.8
C-C	21.6	610	0.812	11.1	–	–	–	–	22.1	614	0.821	11.5
C-N	21.0	610	0.770	10.2	22.7	615	0.784	11.3	–	–	–	–
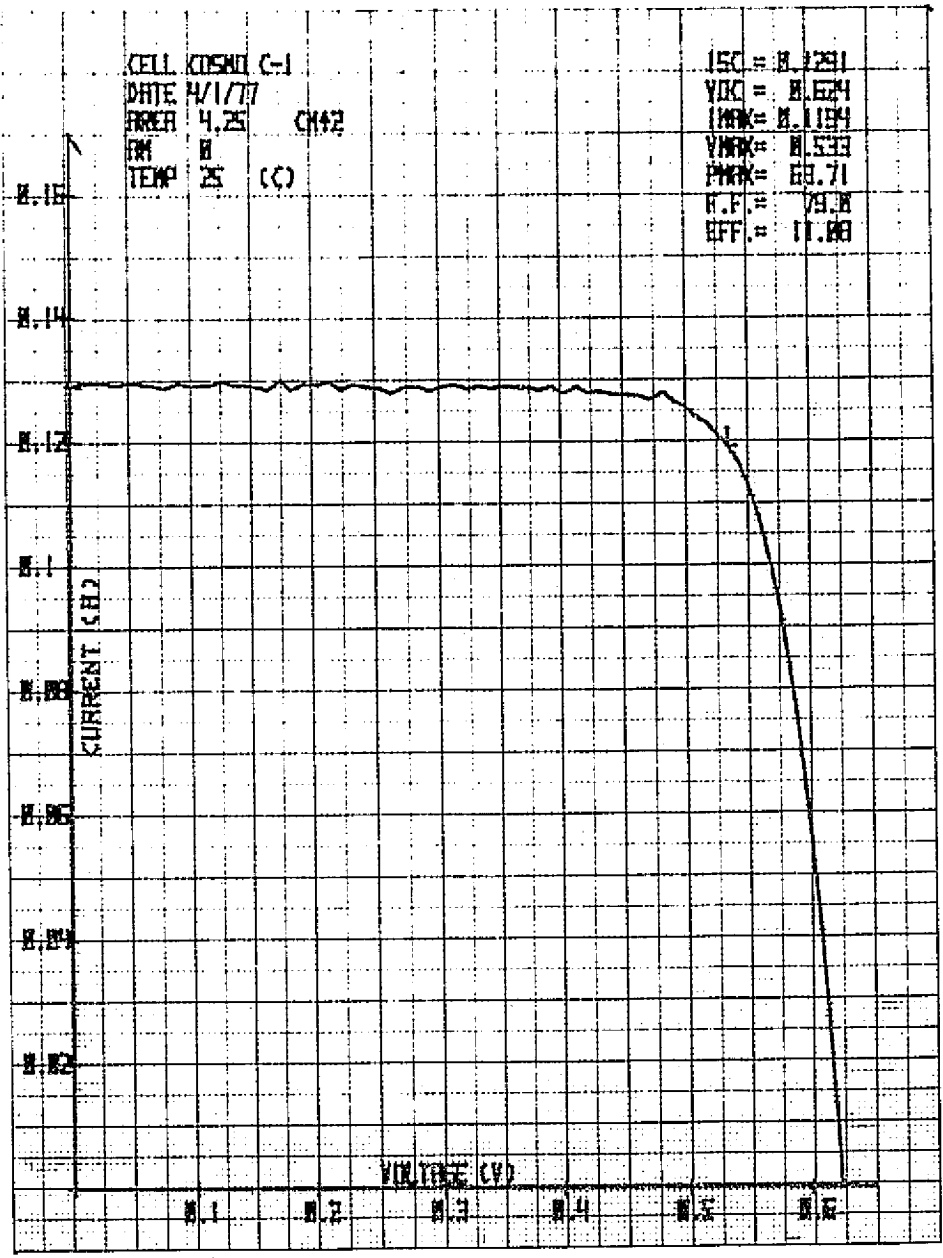
Figure D-1.   Illuminated AM-O responses and parameters measured at
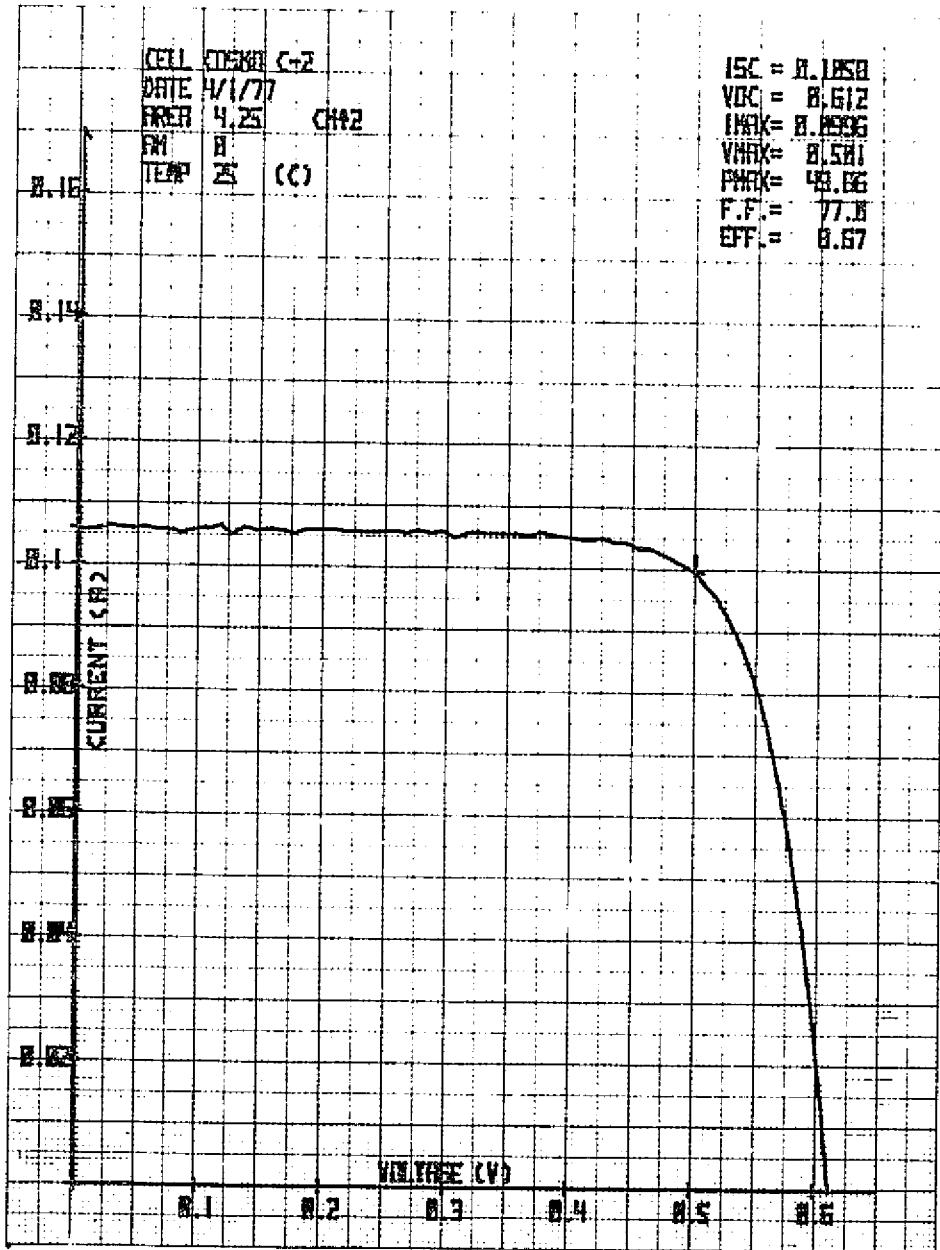NASA-Lewis for sample C-1.

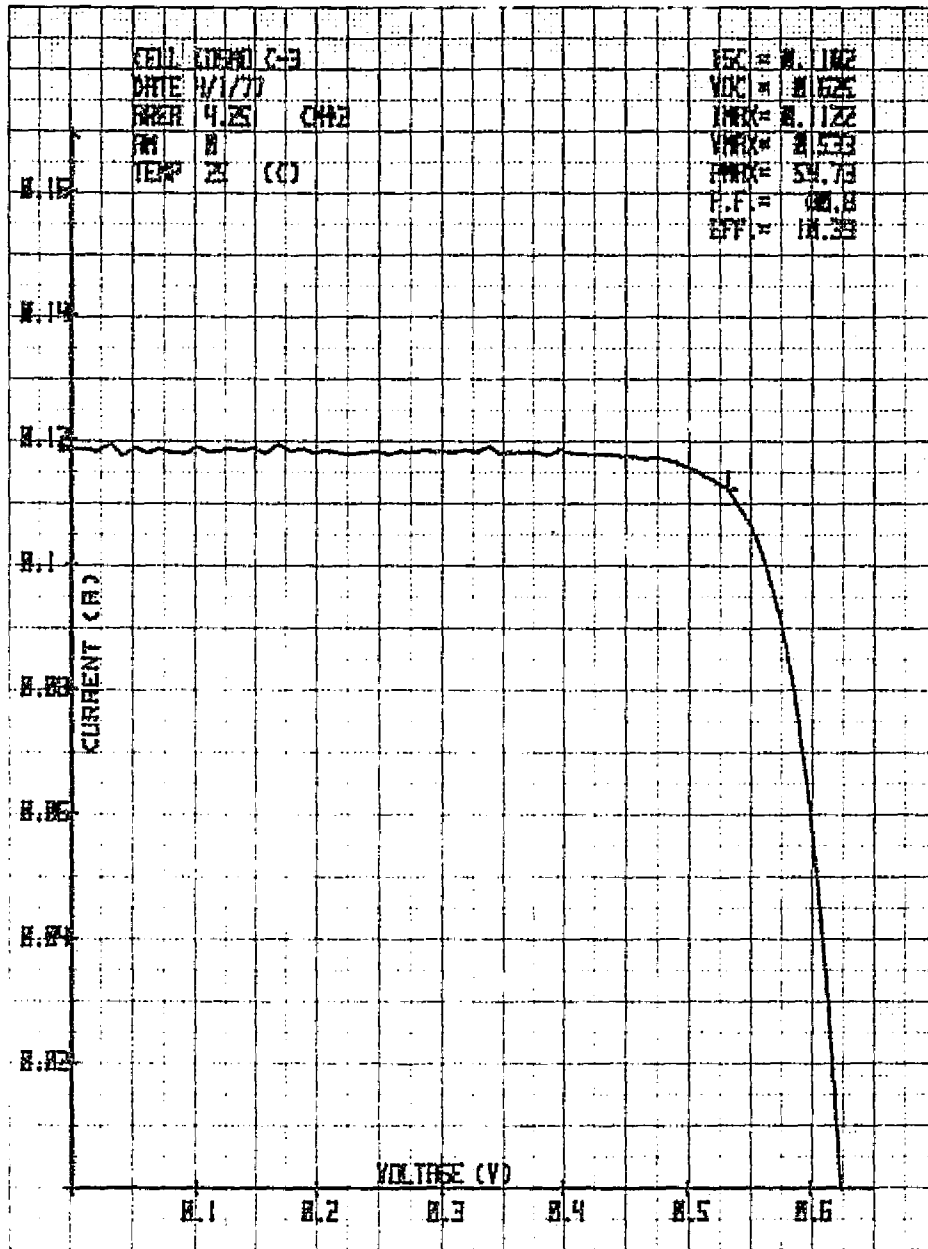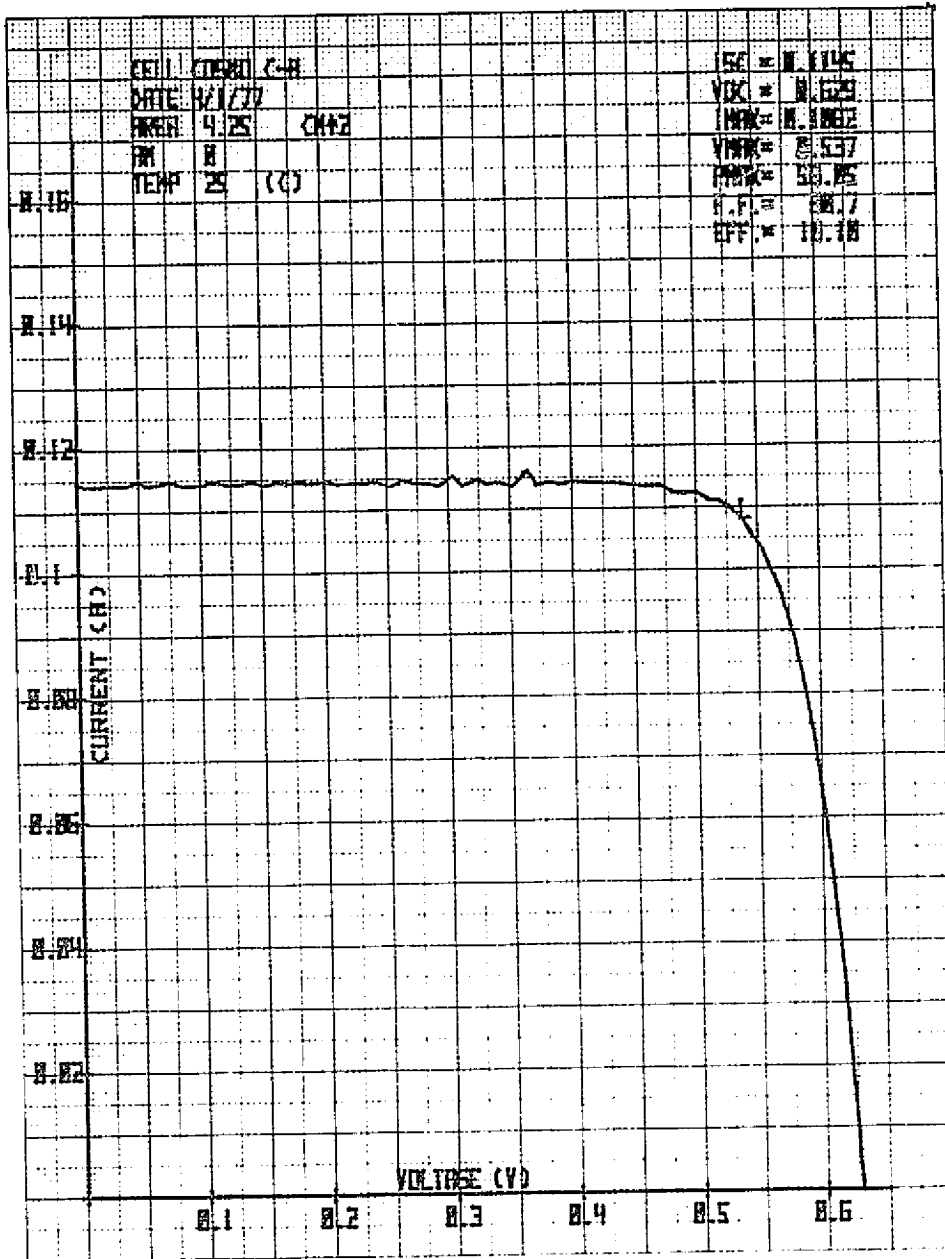Figure D-2. Illuminated AM-0 response and parameters measured at
NASA-Lewis for sample C-2.

Figure D-3. Illuminated AM-O responses and parameters measured at NASA-Lewis for sample C-3.

Figure D-4. Illuminated AM-O responses and parameters measured at
NASA-Lewis for sample C-A.

Figure D-5.   Illuminated AM-O responses and parameters measured at
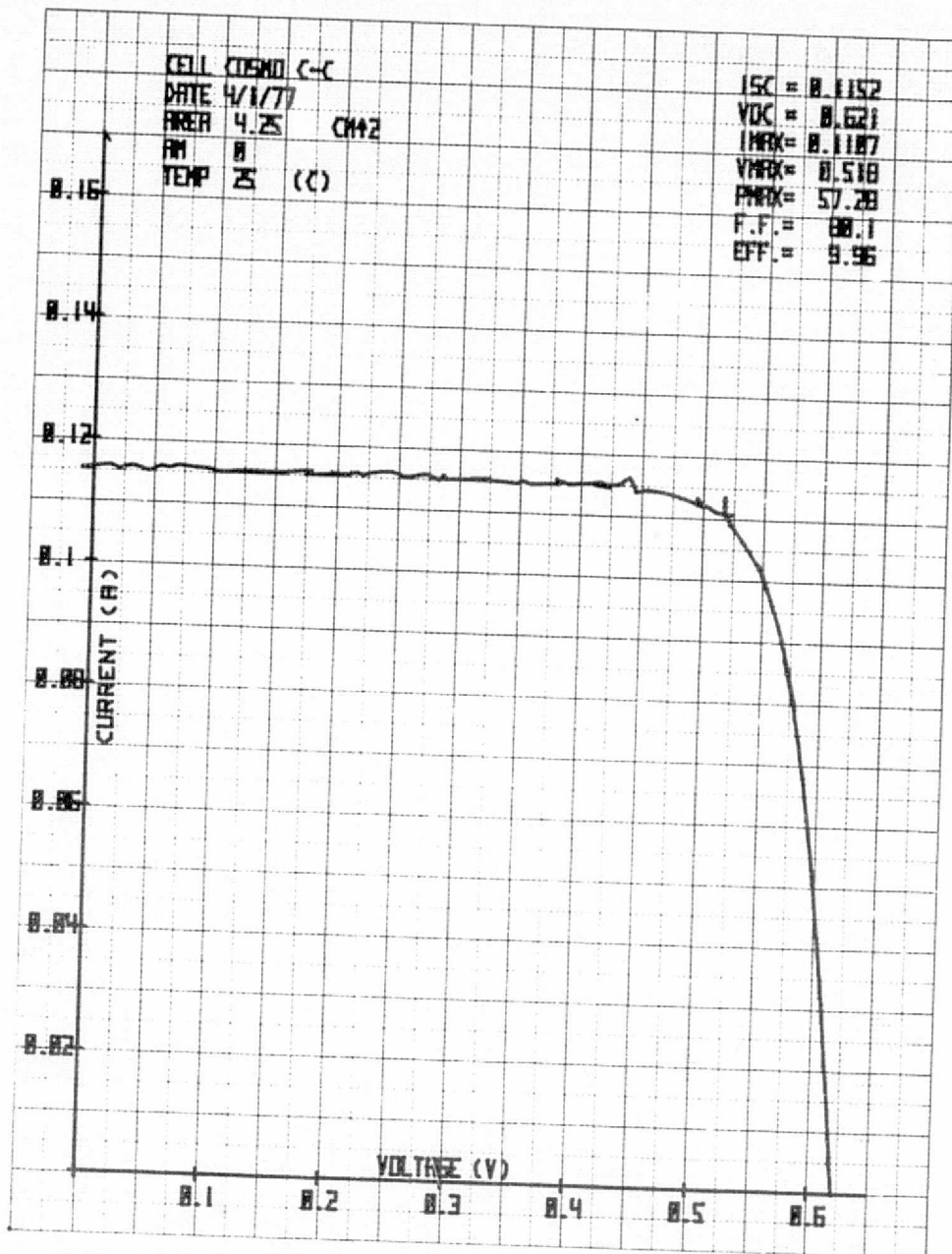NASA-Lewis for sample C-B.

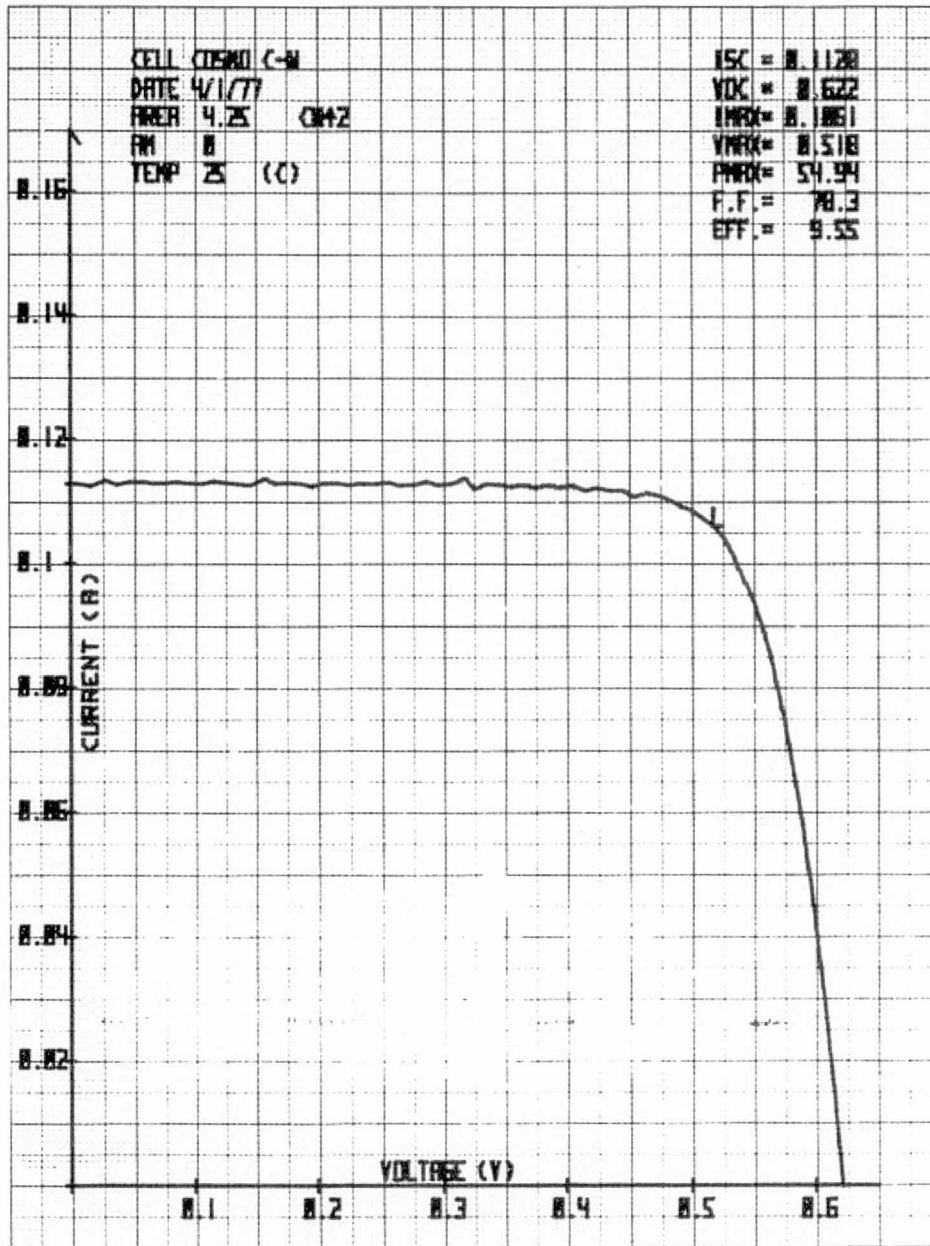Figure D-6. Illuminated AM-0 responses and parameters measured at NASA-Lewis for sample C-C.

Figure D-7. Illuminated AM-O responses each parameters measured at
NASA-Lewis for sample C-N.